Cell Reports
Report

A Presynaptic Role for the Cytomatrix Protein GIT in Synaptic Vesicle Recycling

Jasmin Podufall,[1,4] Rui Tian,[2,5] Elena Knoche,[3] Dmytro Puchkov,[1,4] Alexander M. Walter,[1,2,3] Stefanie Rosa,[1,2] Christine Quentin,[2] Anela Vukoja,[1,4] Nadja Jung,[4] Andre Lampe,[1,4] Carolin Wichmann,[2] Mathias Böhme,[2] Harald Depner,[2] Yong Q. Zhang,[5] Jan Schmoranzer,[1,4] Stephan J. Sigrist,[2,3,*] and Volker Haucke[1,3,4,*]
[1]Leibniz Institute for Molecular Pharmacology, Robert Rössle Strasse 10, 13125 Berlin, Germany
[2]Genetics, Institute for Biology, Freie Universität Berlin, Takustraße 6, 14195 Berlin, Germany
[3]NeuroCure Cluster of Excellence, Charité Universitätsmedizin Berlin, Virchowweg 6, 10117 Berlin, Germany
[4]Membrane Biochemistry, Institute of Chemistry & Biochemistry, Freie Universität Berlin, Takustraße 6, 14195 Berlin, Germany
[5]Institute of Genetics and Developmental Biology, Chinese Academy of Sciences, Beijing 100101, China
*Correspondence: stephan.sigrist@fu-berlin.de (S.J.S.), haucke@fmp-berlin.de (V.H.)
http://dx.doi.org/10.1016/j.celrep.2014.04.051

SUMMARY

Neurotransmission involves the exo-endocytic cycling of synaptic vesicles (SVs) within nerve terminals. Exocytosis is facilitated by a cytomatrix assembled at the active zone (AZ). The precise spatial and functional relationship between exocytic fusion of SVs at AZ membranes and endocytic SV retrieval is unknown. Here, we identify the scaffold G protein coupled receptor kinase 2 interacting (GIT) protein as a component of the AZ-associated cytomatrix and as a regulator of SV endocytosis. GIT1 and its *D. melanogaster* ortholog, dGIT, are shown to directly associate with the endocytic adaptor stonin 2/stoned B. In *Drosophila dgit* mutants, stoned B and synaptotagmin levels are reduced and stoned B is partially mislocalized. Moreover, *dgit* mutants show morphological and functional defects in SV recycling. These data establish a presynaptic role for GIT in SV recycling and suggest a connection between the AZ cytomatrix and the endocytic machinery.

INTRODUCTION

Synaptic transmission involves the rapid calcium-triggered exocytosis of synaptic vesicles (SVs) at presynaptic active zones (AZs) (Gundelfinger and Fejtova, 2012; Haucke et al., 2011) followed by SV protein endocytosis at the rim of the AZ (Dittman and Ryan, 2009; Haucke et al., 2011). The AZ membrane is associated with an electron-dense protein matrix, termed the cytomatrix of the active zone (CAZ), that is partially resistant to detergent extraction (Phillips et al., 2001). CAZ components (Gundelfinger and Fejtova, 2012) include giant multidomain proteins such as piccolo, bassoon, ELKS (also termed CAST), relatives of *Drosophila* bruchpilot (BRP) (Kittel et al., 2006) and Fife (Bruckner et al., 2012), Rab3 interacting molecules (RIMs) (Kaeser et al., 2011), RIM binding proteins (RBPs) (Liu et al., 2011), Munc13, liprins, and G protein coupled receptor kinase 2 interacting protein (GIT) (Kim et al., 2003). Endocytic retrieval of exocytosed SV proteins involves adaptor proteins (Dittman and Ryan, 2009) such as AP-2, stonins (Fergestad and Broadie, 2001; Mullen et al., 2012), and AP180 (Koo et al., 2011). Stonin 2, the mammalian ortholog of *Drosophila* stoned B and of *C. elegans* unc-41 (Mullen et al., 2012), acts as a cargo-specific sorter for the SV calcium sensor synaptotagmin (Diril et al., 2006; Kononenko et al., 2013). The precise location and mechanisms of SV protein recapture and SV reformation remain enigmatic. Based on superresolution imaging, it was suggested that SV protein endocytosis may occur from the periactive zone, a horseshoe-shaped area surrounding the AZ center (Hua et al., 2011). Recent data indicate that SV exocytosis at AZs and SV endocytosis from the periactive zone are functionally coupled (Haucke et al., 2011; Hosoi et al., 2009; Xu et al., 2013). The mechanism that underlies coupling, as well as the physical and functional relationship between the CAZ and the endocytic machinery, is poorly understood.

Here, we establish a presynaptic role for the AZ-associated scaffold protein GIT in SV endocytosis. Mammalian GIT1 harbors a GTPase activating domain for ADP ribosylation factor 6 (Arf6) and among other factors associates with CAZ components (Kim et al., 2003). We show that GIT plays a presynaptic role in stonin-mediated SV recycling, suggesting a physical and functional connection between the presynaptic AZ cytomatrix and the machinery for SV endocytosis. As GIT1 is genetically linked to attention-deficit hyperactivity disorder (ADHD) (Won et al., 2011), these findings are important for our understanding of neurological and neuropsychiatric diseases.

RESULTS

GIT Localizes to the Periphery of Presynaptic AZs and Binds to stonin 2/stoned B

GIT1 is involved in CAZ organization via its association with the AZ protein piccolo (Kim et al., 2003) and regulates endocytic membrane traffic (Claing et al., 2000), suggesting a potential presynaptic function in SV exo-endocytosis. Neither the localization nor the role of GIT1 in the presynapse has been studied so far. We therefore analyzed the localization of GIT1 and the AZ protein

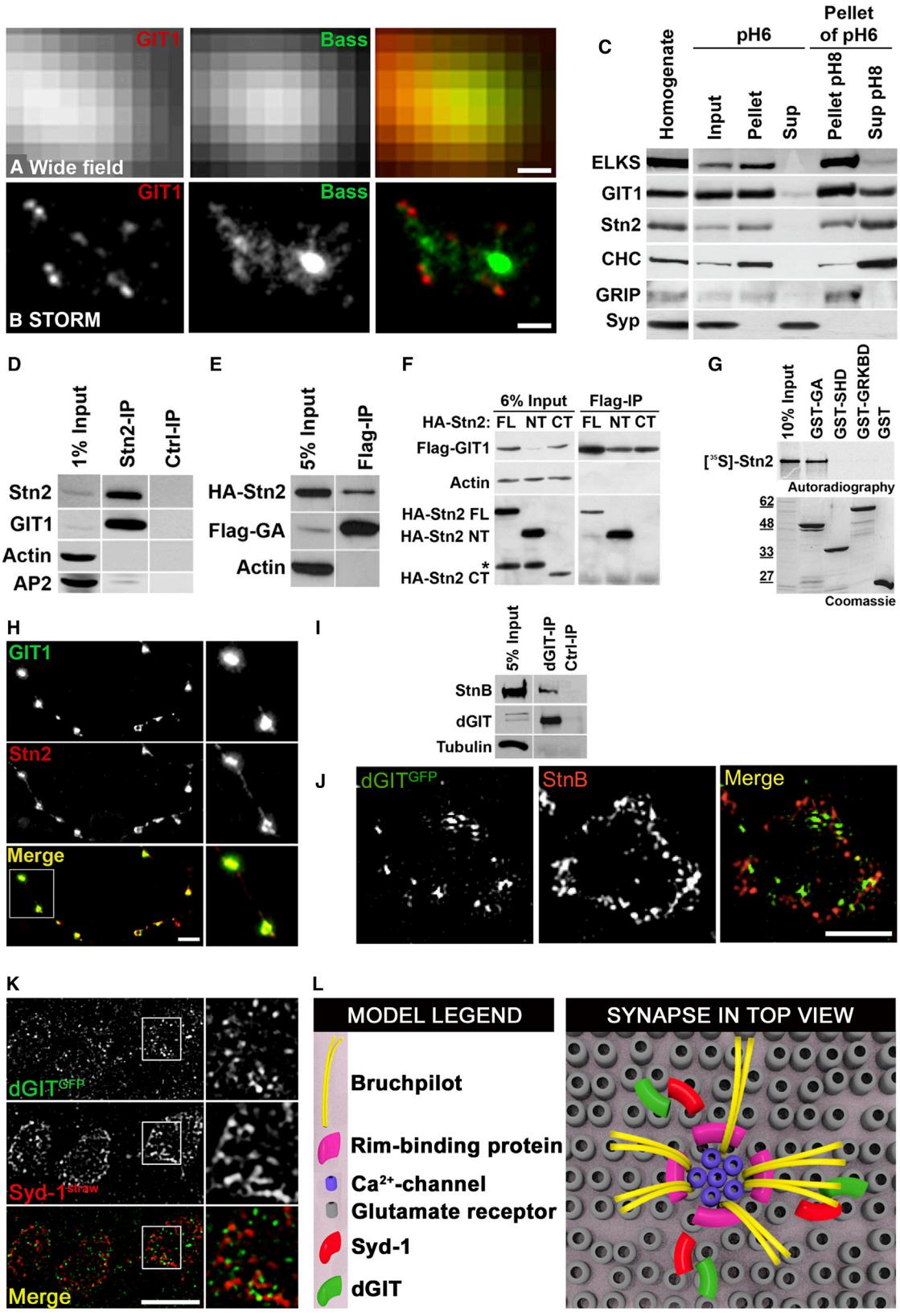

(legend on next page)

bassoon at hippocampal synapses. Since the size of AZs is below the diffraction limit of resolution (Figure 1A), we employed multicolor spectral demixing direct stochastic optical reconstruction microscopy (SD-*d*STORM) with a lateral resolution of 25 nm (Lampe et al., 2012). GIT1 localized to distinctive puncta at the periphery of the AZ center defined by bassoon (Figure 1B), with a mean peak distance between individual bassoon spots and GIT1 of 76 ± 8 nm (SEM, n = 30 synapses), which is similar to that measured by STORM for bassoon and the AZ protein RIM1 (mean ± SEM ~40 ± 5 nm), but much smaller than the distance between bassoon and the postsynaptic protein Homer1 (mean ± SEM ~154 ± 1.2 nm) (Dani et al., 2010). To confirm the association of GIT1 with the CAZ, we used a biochemical approach for the enrichment of detergent-resistant proteins that may represent a biochemical correlate of the CAZ (Phillips et al., 2001). Detergent extraction of synaptosomes at pH 6 renders the majority of pre- and postsynaptic scaffolds, including CAZ components, insoluble. Re-extraction at elevated pH partially solubilizes proteins of the presynaptic CAZ. As expected for CAZ components, the majority of GIT1 and the BRP-related AZ protein ELKS remained detergent insoluble at pH 6, whereas the SV protein synaptophysin was solubilized completely (Figure 1C). Re-extraction of the insoluble pH 6 pellet at pH 8 solubilized a small fraction of GIT1 and ELKS, whereas postsynaptic GRIP remained insoluble (Figure 1C). Thus, GIT1 exhibits a partitioning behavior similar to that of the known AZ protein ELKS, confirming its association with the CAZ at mammalian synapses.

To further dissect a presynaptic role for GIT1 in SV exo-endocytosis, we aimed to identify presynaptic binding partners. Because reliable anti-GIT1 suitable for immunoprecipitation were unavailable, we screened a variety of well-characterized antibodies against known presynaptic proteins for their ability to coimmunoprecipitate GIT1 using tandem mass spectrometry (MS/MS)-based proteomics as a readout. These experiments identified GIT1 as a possible binding partner of the endocytic adaptor stonin 2 (Figure 1D). Further biochemical analysis using different truncation mutants (Figure S1G) revealed that the interaction between stonin 2 and GIT1 is direct (Figure 1G) and mediated by the ArfGAP-ankyrin repeat domain of GIT1 (Figures 1E and S1A) and the N-terminal domain (NT, aa 1–555) of stonin 2 (Figure 1F). Further, the conserved stonin-homology domain (StHD, aa 411–553) of stonin 2 on its own was unable to bind to GIT1, as was the related nonneuronal protein stonin 1 (Figures S1A and S1B). When expressed in mammalian cells, stonin 2-NT also bound to GIT2, but was unable to associate with non-GIT family ArfGAPs such as ACAP1 (Figure S1C). We observed no significant effects of stonin 2 on the ArfGAP activity of GIT1 (Figure S1H), suggesting that the GIT-stonin complex may serve a structural rather than an enzymatic role. We also probed whether complex formation between GIT and stonin family members is evolutionarily conserved. dGIT coimmunoprecipitated with the sole stonin family protein, stoned B, from *Drosophila* head extracts (Figure 1I), and this association was mediated by the ArfGAP-ankyrin repeat domain of dGIT (Figure S1D), similar to what was observed for mammalian GIT1. The evolutionary conservation of complex formation between GIT and stonin is underscored by the ability of *Drosophila* stoned B to bind to human GIT1 (Figure S1E) and of dGIT to associate with human stonin 2-NT (Figure S1F).

To corroborate these biochemical data, we studied the localization of GIT and stonin 2/stoned B in primary hippocampal neurons and at *Drosophila* larval neuromuscular junctions (NMJs). In hippocampal neurons in culture, GIT1 was concentrated at and around bassoon-containing presynaptic sites (Figure S1I), where it colocalized with stonin 2 (Figure 1H). Moreover, stonin 2 together with GIT1 and the endocytic protein clathrin (Phillips et al., 2001) partitioned to the detergent-insoluble CAZ in biochemical fractionation experiments (Figure 1C). Superresolution, dual-color, structured illumination microscopy imaging of *Drosophila* larval NMJs showed endogenous stoned B to be closely apposed to transgenically expressed dGIT-GFP (a construct that rescues dGIT loss of function [see below]; Figure 1J). To precisely define the localization of dGIT with respect to the AZ, we used dual-color stimulated emission depletion (STED) nanoscopy with a lateral resolution of 20 nm (Göttfert

Figure 1. GIT Localizes to the Edge of AZs and Directly Binds to stonin 2/stoned B

(A and B) GIT1 localizes to distinctive puncta at the periphery of the AZ center. Cultured hippocampal neurons (DIV14) costained for GIT1 (red) and bassoon (Bass, green) shown in wide field (A) or SD-*d*STORM (B). Scale bars, 200 nm.

(C) GIT1 is part of a detergent-resistant presynaptic matrix. Synaptosomes were extracted with 1% Triton X-100 at pH 6. The insoluble pellet was re-extracted with 1% Triton X-100 at pH 8. Equal amounts of soluble material (sup) and insoluble material (pellet) were analyzed by immunoblotting against the AZ protein ELKS, GIT1, stonin 2 (Stn2), clathrin heavy chain (CHC), synaptophysin (Syp), or the postsynaptic scaffold GRIP.

(D) Analysis of immunoprecipitates with antibodies against stonin 2 (Stn2), GIT1, actin, or AP2 (negative controls). GIT1 was coimmunoprecipitated with anti-Stn2 antibodies (Stn2-IP), but not control immunoglobulin G (IgG; Ctrl-IP).

(E) The FLAG-tagged ArfGAP-ankyrin repeat domain (GA) of GIT1 coimmunoprecipitates hemagglutinin-Stn2 (HA-Stn2) from transfected Cos7 cells.

(F) GIT1 associates with the NT domain of Stn2 in immunoprecipitates. FL, Stn2-full length; CT, Stn2 C-terminal domain.

(G) In vitro-translated Stn2 directly binds to the GA domain of GIT1. GST-GIT1 truncation mutants (GA, Spa2 homology domain [SHD], and G protein receptor kinase binding domain [GRKBD]) were used to pull down in vitro-translated [^{35S}]-Stn2.

(H) Colocalization of endogenous GIT1 (green) with HA-tagged stonin 2 (Stn2, red) at synapses of primary hippocampal neurons in culture (DIV14). Scale bar, 5 μm.

(I) Coimmunoprecipitation of dGIT with stoned B (StnB) from *D. melanogaster* head extracts using dGIT antibodies (dGIT-IP). Ctrl-IP, preimmune IgG.

(J) StnB is closely apposed to transgenically expressed dGIT-GFP at *Drosophila* larval NMJs. dGIT-GFP-expressing NMJs were immunostained with antibodies against StnB and GFP and imaged by structured illumination microscopy. Scale bar, 2 μm.

(K) Single-layer STED images showing the localization of dGit^{GFP} in relation to Syd-1^{straw} at the *Drosophila* larval NMJ. *Anti*-GFP and *anti*-DsRed immunoreactivity was observed in close proximity to each other, indicating that dGIT is positioned in the periphery of the AZ. Scale bar, 2 μm.

(L) Model of an AZ in top view, showing the position of the indicated proteins in relationship to each other.

See also Figure S1.

et al., 2013). STED-based nanoscopy revealed dGIT to be localized to the rim of presynaptic AZs closely interspaced with Syd-1, a scaffold of the AZ periphery surrounding BRP at the AZ center (Owald et al., 2010; Figures 1K and 1L). Thus, the precise localization of GIT at both glutamatergic hippocampal synapses and glutamatergic *Drosophila* NMJs appears very similar. These results show that GIT and stonin 2/stoned B associate with the CAZ, directly bind to each other, and localize to the periphery of AZs at presynaptic sites.

GIT Regulates the Localization and Function of stonin 2/stoned B at Synapses

Mammalian genomes contain two similar GIT genes (encoding GIT1 and GIT2) that likely overlap functionally. Moreover, mammalian GIT1 regulates synapse formation and postsynaptic spine morphogenesis (Menon et al., 2010; Segura et al., 2007), compromising analysis of a possible presynaptic function of GIT1/2 in vivo. To circumvent these problems when analyzing the role of GIT at the presynapse in vivo, we decided to subject the single *Drosophila dgit* locus to genetic manipulation (Figure S2A). Using transposon-mediated excision, we deleted major parts of dGIT (eliminating expression of the Spa2 homology domain [SHD] and paxillin-binding site [PBS] domain) together with the neighboring gene (CG11833; Figure S2A). To remove dGIT function from flies, we placed the resulting chromosome (*dgitex10*) over a piggy Bac transposon insertion located within the dgit locus (dgitf03586). In the resulting transheterozygous mutants (dgitex10/dgitf03586; hereafter referred to as *dgit f03*), dGIT function was specifically eliminated. A second dGIT loss-of-function mutant was generated by placing *dgitex10* over a large deficiency Df(2R)Df596 (*dgitex10*/Df(2R)Df596; referred to as *dgit Df*). Both mutants displayed undetectable dGIT protein expression in fly head extracts (Figure 2A) and reduced adult viability (not shown). Moreover, locomotion assessed by negative geotaxis was similarly affected in both alleles (*dgit Df* and *dgit f03*; Figure 2B). Importantly, these phenotypes were rescued by transgenic neuronal (e.g., presynaptic) re-expression of dGIT or GFP-dGIT under the panneuronal *elav-Gal4* driver (see Figure 2B and below). Thus, defects in locomotion can be assigned to a loss of dGIT function in the nervous system and specifically within the presynaptic compartment.

The physical association of dGIT with stoned B suggests a possible functional relationship between the two proteins. Quantitative immunoblotting revealed that stoned B levels were significantly reduced in head extracts from *dgit f03* mutant animals, whereas expression of other endocytic proteins, such as Dap160/intersectin and dynamin, were unaltered (Figures 2C–2F). To probe whether similar alterations may occur at the level of presynaptic boutons, we analyzed the expression or localization of synaptic proteins at *Drosophila* larval NMJs. Quantification of the levels of various pre- and postsynaptic proteins in *dgit* mutant NMJs revealed a significant and specific decrease in the amount of stoned B, a phenotype that was fully rescued by presynaptic re-expression of dGIT. In contrast, no change in the amount of the endocytic protein Dap160/intersectin was found in either genotype (Figures 2G–2I). We then analyzed the localization and expression of the SV proteins CSP and synaptotagmin 1, the AZ protein BRP, and postsynaptic glutamate receptors (Figure S2B). Stoned B has previously been shown to be required for proper expression and endocytic sorting of synaptotagmin in flies and mammals (Diril et al., 2006; Fergestad and Broadie, 2001; Stimson et al., 2001). Presynaptic expression of synaptotagmin 1 was indeed reduced in *dgit* mutants compared with controls, akin to what was observed for stoned B mutants (Fergestad and Broadie, 2001; Stimson et al., 2001), and this was rescued by re-expression of dGIT (Figures 2J and S2B). By contrast, the levels of CSP or BRP were unaltered in *dgit* mutant animals (Figures 2K, 2M, and S2B). Endocytic missorting of synaptotagmin, similar to loss of function of stoned B in *Drosophila* or of stonin 2 in mice (Kononenko et al., 2013), was also observed in hippocampal neurons expressing synaptotagmin 1-pHluorin depleted of endogenous GIT1 by small interfering RNA (siRNA; Figures S4D and S4E). Thus, the function of the dGIT/GIT1-stoned B/stonin 2 complex seems to be evolutionarily conserved. Postsynaptic glutamate receptor fields were enlarged in *dgit* mutant NMJs, a phenotype rescued by motoneuron-specific re-expression of dGIT (Figures 2L and S2B). A similar enlargement of glutamate receptor fields (juxtaposed with presynaptic AZs) was observed previously in other mutants that affect CAZ integrity (e.g., *syd-1* and *brp*) (Kittel et al., 2006; Owald et al., 2010).

Loss of *dgit* not only resulted in reduced presynaptic expression of stoned B but also caused a partial, yet significant redistribution of stoned B from cortical areas of presynaptic boutons toward the lumen, indicating that dGIT regulates proper subsynaptic targeting of stoned B (Figures S2C and S2D), whereas Dap160/intersectin distribution appeared unaffected. These results show that GIT regulates the localization and function of stonin 2/stoned B at synapses.

Accumulation of Enlarged Vesicles at *dgit* Mutant Synapses

Drosophila stoned mutants not only display defects with respect to synaptotagmin expression but also show morphological abnormalities within their NMJs, most notably an accumulation of enlarged (>100 nm) endocytic vesicles (Fergestad and Broadie, 2001; Stimson et al., 2001). To probe for possible ultrastructural alterations during SV cycling, we stimulated wild-type (WT) or *dgit f03* mutant larvae and, following a brief period of recovery, analyzed their presynaptic ultrastructure by electron microscopy (EM)-based morphometry. Synapses from *dgit* mutants appeared largely unaltered (Figures 3A–3D), with no change in the numbers of SVs (Figure 3E) or SVs docked to the presynaptic membrane (Figure 3F). Moreover, *dgit* mutants displayed a normal size (Figure 3G) and structure of the CAZ, as well as a normal organization of T-bars (Figures 3C and 3D) and the SVs tethered to them (Figures 3C–3F). However, *dgit* mutant terminals showed an accumulation of endosomal structures and vacuoles (i.e., >80 nm vesicles or cisternae; Figures 3A–3D and 3H; Table S1) similar to the cisternae observed in *stoned* and in *shibire*^{ts} mutants following release from temperature block. The increased endosome area per bouton was rescued completely by neuron-specific re-expression of dGIT ([in $\mu m^2/\mu m^2$]: control: 0.020 ± 0.004; *dgit f03*: 0.039 ± 0.008*, $p \leq 0.04$; *dgit f03*-rescue: 0.023 ± 0.005, insignificantly different from control), indicating that the defect originates from presynaptic loss of dGIT (Figure 3H).

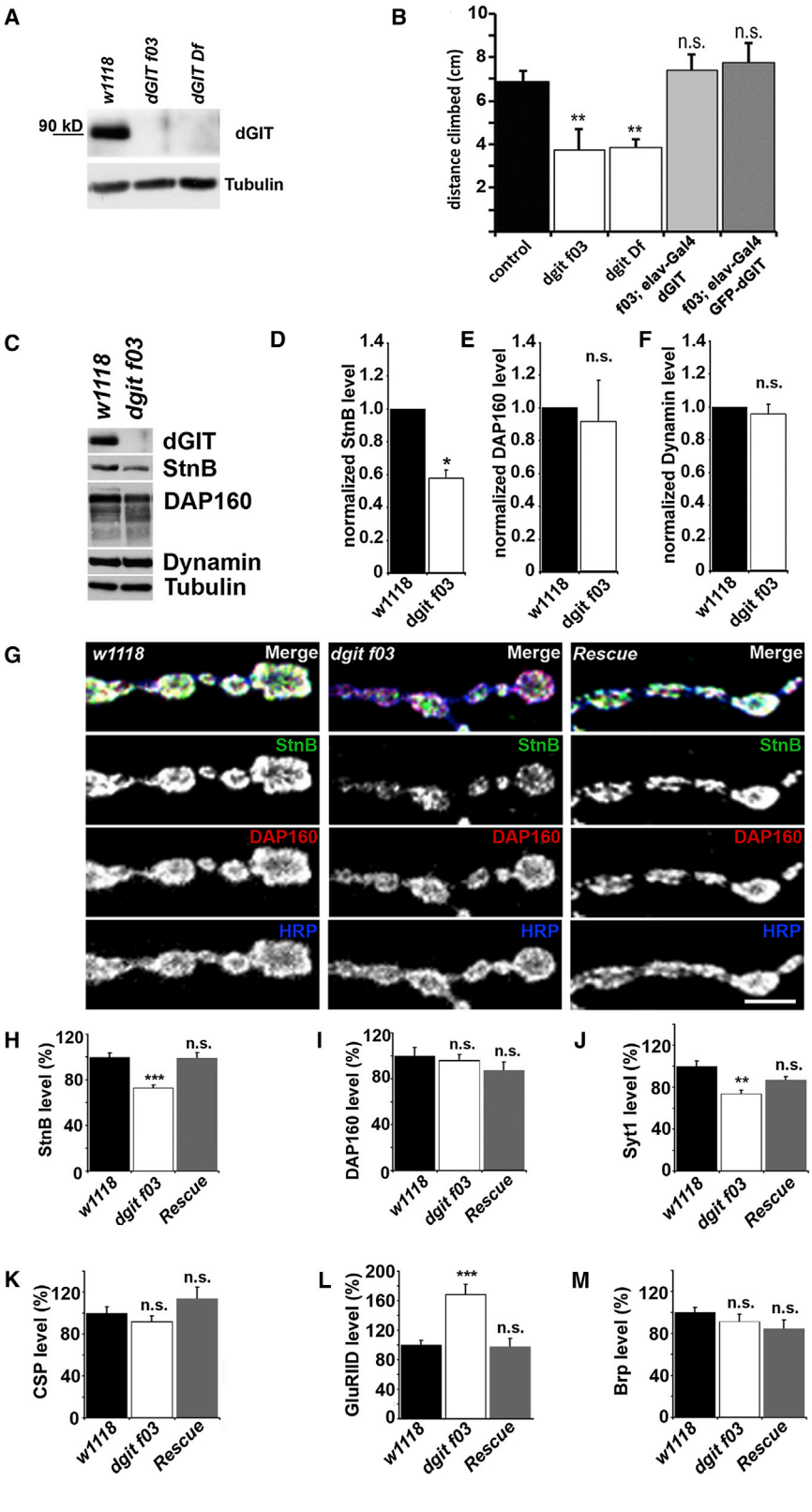

Figure 2. dGIT Regulates Presynaptic Levels and Localization of Stoned B and Synaptotagmin 1 at *Drosophila* NMJ Synapses

(A) Immunoblot analysis of fly head lysates. dGIT is present in WT (w^{1118}/*elav-Gal4*) but undetectable in *dgit* mutants (*Dgit Df: elav-Gal4/+*; *dgitDf596/10* and *Dgit f03: elav-Gal4/+*; *f03568/10*). Tubulin, control.

(B) Locomotion was analyzed in control w^{1118}/*elav-Gal4*, *dgit* mutants, and *rescue* adult flies after the flies' wings were clipped. *dgit f03* and *Df* mutants showed decreased negative geotaxis as quantified by the mean distance climbed vertically within 30 s. Control: w^{1118}/*elav-Gal4* (n = 24). *Dgit Df*: *elav-Gal4/Y*; *dgitDf596/10* (n = 15). *Dgit f03*: *elav-Gal4/Y*;*dgitf03586/10* (n = 14). *f03;UAS dgit*: *elav-Gal4/Y*; *dgit10/f03586; UAS-dGIT/+* (n = 10). *f03;UAS GFP-dgit*: *elav-Gal4/Y*; *dgit10/f03586; UAS-GFP::dGIT/+* (n = 9; mean ± SEM).

(C–F) Reduced levels of stoned B (StnB) in head extracts from *dgit f03* mutant flies.

(C) Fly head extracts (five heads per lane) from adult w^{1118}/*elav-Gal4* or *dgit* mutants flies (*dgit f03[elav-Gal4/+; f03568/10]*) were analyzed by quantitative immunoblotting against the indicated proteins.

(D–F) StnB is reduced (D; *dgit f03*: 0.58 ± 0.05, p = 0.0132), whereas Dap160/intersectin (E; *dgit f03*: 0.91 ± 0.25, p = 0.7691, n.s.) and dynamin (F; *dgit f03*: 0.96 ± 0.06, p = 0.5528, n.s.) are unchanged (mean ± SEM, n ≥ 2 experiments).

(G) StnB levels are reduced at dGIT mutant NMJs, a phenotype rescued by presynaptic reexpression of dGIT. Muscle 4 NMJ from WT (w^{1118}), dGIT mutant (*dgit f03*), and *dgit rescue* larvae immunostained for StnB (green), Dap160/intersectin (red), and horseradish peroxidase (blue) are shown. Scale bar, 4 μm.

(H and I) Quantification of data in (G). The levels of StnB are significantly decreased in *dgit* mutants (H; w^{1118}: 100 ± 3.7, n = 28; *dgit f03*: 73.1 ± 2.5, n = 31, p < 0.0001; *rescue*: 98.8 ± 5.1, n = 19, p = 0.847), whereas Dap160/intersectin remains unchanged (I; w^{1118}: 100 ± 7.4, n = 17; *dgit f03*: 96.3 ± 4.9, n = 22, p = 0.671; *rescue*: 87.4 ± 7.3, n = 14, p = 0.242). Mean ± SEM.

(J–M) Quantification of pre- and postsynaptic protein levels at NMJs from WT (w^{1118}), dGIT mutant (*dgit f03*), and *dgit rescue* larvae. Levels of synaptotagmin 1 (Syt1) are reduced in *dgit* mutants (J; w^{1118}: 100 ± 4.9, n = 18; *dgit f03*: 73.7 ± 3.6, n = 17, p = 0.0002; *rescue*: 86.5 ± 3.7, n = 12, p = 0.056). Levels of CSP (K; w^{1118}: 100 ± 6.1, n = 30; *dgit f03*: 92.2 ± 5.2, n = 27, p = 0.340; *rescue*: 113.8 ± 11.2, n = 28, p = 0.276) or Brp (M; w^{1118}: 100 ± 4.6, n = 19; *dgit f03*: 91.0 ± 7.2, n = 20, p = 0.306; *rescue*: 84.1 ± 8.7, n = 18, p = 0.108) are unchanged, whereas glutamate receptor (GluRIID) levels are increased (L; w^{1118}: 100 ± 5.9, n = 15; *dgit f03*: 168.6 ± 13.6, n = 17, p = 0.0001; *rescue*: 97.4 ± 11.2, n = 15, p = 0.843). Mean ± SEM. Scale bar, 4 μm.

See also Figure S2.

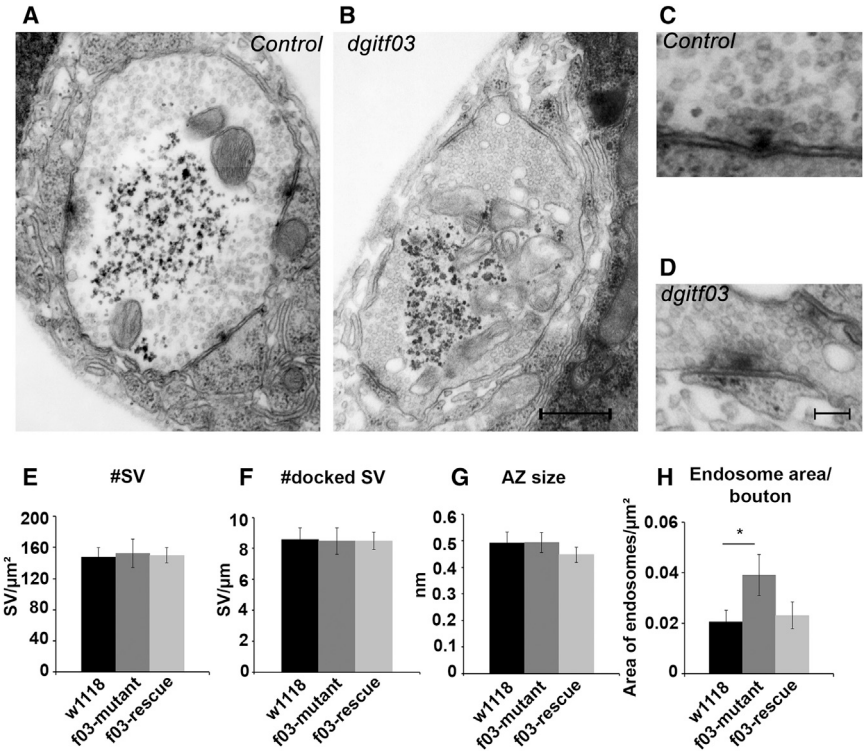

Figure 3. Accumulation of Endosomal Structures at *dgit* Mutant Synapses

Ultrastructure of *Drosophila* type 1b NMJs from larvae that were stimulated in 60 mM, KCl/5 mM $CaCl_2$ for 5 min and then recovered for 5 min to allow for SV reformation.

(A–D) Synapse structure, including the SV number, docked SV number, and AZ size, is unaltered in *dgit* mutants (B and D) compared with controls (A and C) or rescued animals (*dgit rescue*; E–H). T-bar morphology is unaffected (C and D).

(E–H) No significant changes in SV numbers per bouton area (E), docked SV numbers per AZ length (F), or AZ size (G) are seen. Stimulated *dgit f03* mutants display an elevated number of endosomal structures (quantified as sum area of endosomal profiles defined as >80 nm vesicles or cisternae normalized to the total bouton area), a phenotype rescued by transgenic reexpression of dGIT (H). The ≥20 boutons were analyzed with at least 6 larvae per genotype (mean ± SEM). Scale bars, 500 nm in (B) and 150 nm in (D). See also Figure S3.

To explore whether these ultrastructural alterations in *dgit* mutants are linked to functional deficits in neurotransmission, we performed two electrode voltage-clamp recordings of late third-instar larval NMJs. Evoked excitatory junctional currents (eEJCs) were significantly reduced in *dgit f03* mutant larvae compared with controls, a defect that was rescued by presynaptic re-expression of UAS-*dgit* using the motoneuronal driver *ok6-GAL4* (Figure S3A). No significant changes in the rise times and decay constants τ of evoked responses or in the amplitude of spontaneous miniature currents were observed (Figures S3B and S3C), whereas mEJC frequency was slightly but insignificantly increased (Figure S3D). The mEJC rise time and decay constant τ were also unaltered in *git f03* mutants (mEJC rise time, control: 0.85 ± 0.05, n = 13; *dgit f03*: 0.78 ± 0.05, n = 11; p = 0.31; Student's t test; mEJC τ, control: 7.6 ± 0.5, n = 13; *dgit f03*: 7.3 ± 0.5, n = 11; p = 0.77; Student's t test). Overall, these data show that loss of *dgit* phenocopies the ultrastructural and functional defects observed in *stoned* mutants, further supporting the close physical and functional association of both proteins within the SV cycle.

dGIT Regulates SV Recycling

To probe the putative function of dGIT in SV cycling more directly, we stimulated larval NMJs under depolarizing conditions and monitored SV endocytosis using the styryl dye FM1-43. The amount of FM1-43 that is incorporated serves as a measure for the efficacy of membrane retrieval and thus SV recycling (Verstreken et al., 2008). Control boutons revealed strongly incorporated FM dye, whereas *dgit f03* or *dgit Df* mutant boutons loaded FM1-43 with a significantly reduced efficiency. This apparent defect in SV recycling was rescued by presynaptic re-expression of dGIT (Figures 4A–4G). To dissect a primary role of dGIT in exocytosis from a function in endocytic membrane retrieval, we measured evoked neurotransmission and FM1-43 uptake under conditions of elevated extracellular calcium, which invariably results in a high release probability (Miśkiewicz et al., 2011). Under these conditions, evoked neurotransmission of *dgit f03* mutants did not differ significantly from that of WT controls, whereas FM1-43 uptake was significantly reduced (Figures S4A and S4B), suggesting that defective FM1-43 uptake primarily results from impaired endocytosis or SV recycling.

To further characterize the role of dGIT in SV endocytosis, we transgenically expressed synapto-pHluorin, a chimeric SV protein whose fluorescence is low in the acidic environment of the SV lumen and high when it is exocytosed to the cell surface (Miesenböck et al., 1998). The WT controls and *dgit f03* mutant animals showed identical synapto-pHluorin expression, as revealed by quantification of synaptic fluorescence levels following application of ammonium chloride to alkalize the lumen of SVs (Figure S4C). To systematically investigate possible endocytosis defects, we stimulated exo-endocytosis with action potential (AP) trains at different frequencies (10 Hz and 50 Hz), which invariably resulted in a transient rise and subsequent decay of synapto-pHluorin fluorescence in synaptic boutons. Experiments were performed in 5 mM extracellular $CaCl_2$, which ensured a similar extent of stimulus-induced exocytosis (normalized maximal fluorescence following blockage of SV reacidification with folimcyin: 100 APs at 10 Hz: control = (100 ± 10)%, *dgitf03* = (101 ± 6)%; 100 APs at 50 Hz: control = (100 ± 20)%, dgitf03 = (105 ± 25)%, n = 3 animals and n = 15 boutons), allowing us to study a possible involvement of dGIT in SV endocytosis and postendocytosis processing of internalized membranes independent of its function in exocytosis (see above). Strikingly,

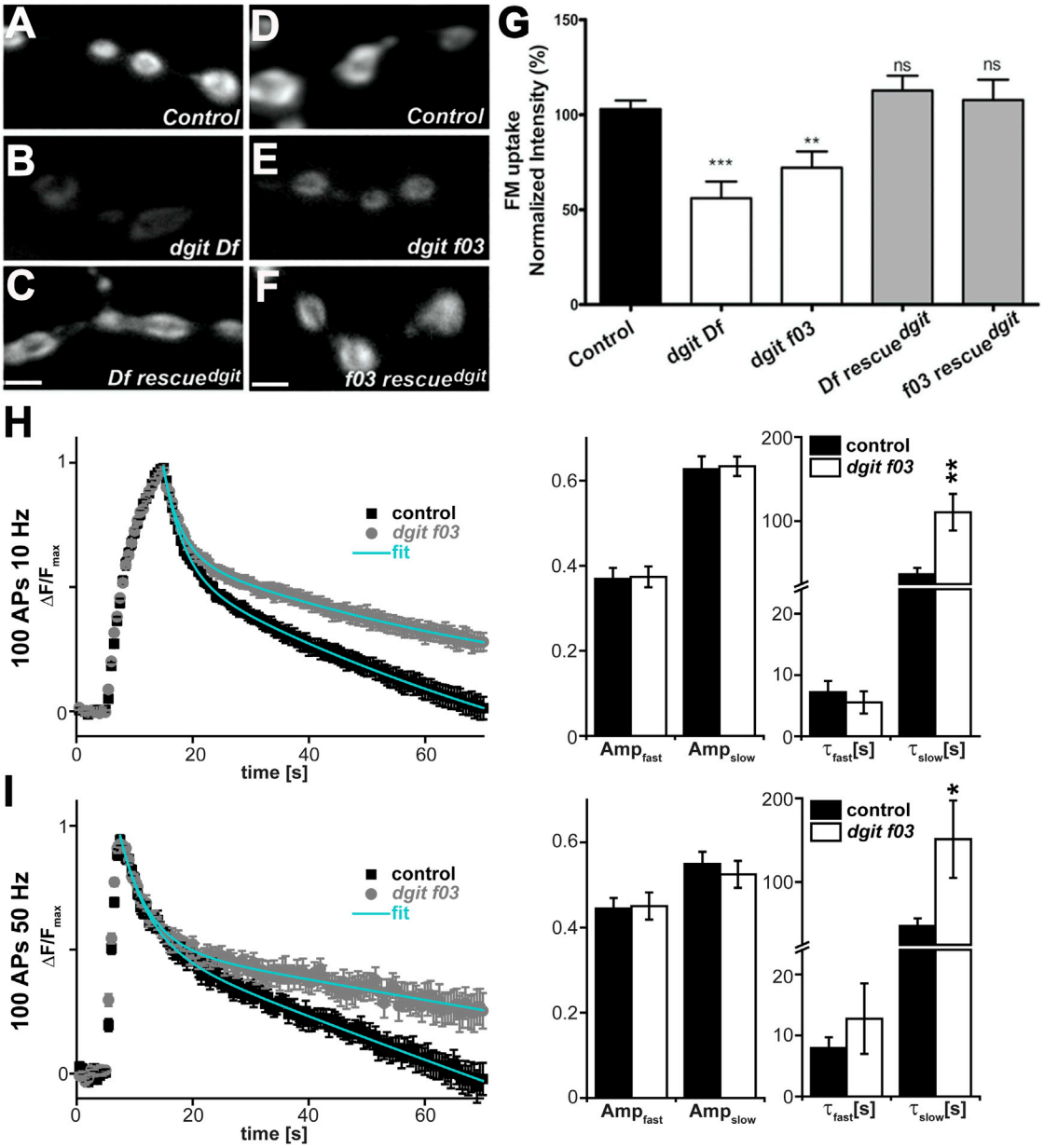

Figure 4. dGIT Regulates SV Recycling

(A–F) FM dye uptake is reduced in *dgit* mutants. FM1-43 dye uptake in control (*w1118*/OK6-Gal4; A and D), *dgit* mutants (*dgit f03* and *dgit Df*; B and E), and the corresponding rescued larvae (*f03 rescue*^{dgit} or *Df rescue*^{dgit}; C and F). Third instar larval NMJs were incubated in 4 μM FM1-43 and stimulated for 5 min with 90 mM KCl, 1.5 mM $CaCl_2$. Scale bar, 2 μm.

(G) Quantification of FM1-43 dye uptake (mean ± SEM, n ≥ 12 NMJs). Student's t test, **p < 0.01, ***p < 0.001; ns, not significant.

(H) Left: exo-endocytosis and vesicle reacidification assayed by synaptopHluorin (SpH). Time-dependent fluorescence changes in response to stimulation with 100 APs at 10 Hz (starting at t = 5 s) in control (black, *OK6*/+; *UAS-SpH*/+) and *dgit f03* (gray, *fo3*/*ex10,OK6*; *UAS-SpH*/+) boutons. The cyan trace is a fit with a double exponential function. Right: kinetic analysis of the bimodal endocytosis/reacidification assayed by SpH. The relative contributions of the fast (Amp_{fast}) and slow (Amp_{slow}) components, as well as the respective time constants (τ_{fast} and τ_{slow}), are shown.

(I) Same as (H), but for a stimulation of 100 APs at 50 Hz. Data in (H) and (I) are mean ± SEM from n ≥ 4 animals with 5 boutons per animal; *p < 0.05, **p < 0.01, two-tailed t test.

See also Figure S4.

normalized fluorescence traces revealed a slowing of the average synapto-pHluorin fluorescence decay in *dgit* mutants (Figures 4H and 4I). To scrutinize this effect further, we investigated the temporal properties of the postexocytosis synapto-pHluorin signals. Fitting of exponentials revealed that the fluorescence decay in both genotypes was well described by a

double exponential function (cyan lines in Figures 4H and 4I), indicative of bimodal kinetics with a fast and a slow component. Quantification of parameters obtained by kinetic analysis of traces from individual boutons revealed that the relative amplitudes of the fast and slow components (Amp_{fast} and Amp_{slow}, respectively, in Figures 4H and 4I) were indistinguishable between control and mutant synapses. Moreover, no significant difference between the fast time constants (τ_{fast} in Figures 4H and 4I) was found, suggesting that this component functions independently of dGIT. In contrast, the time constant of the slow component (τ_{slow} in Figures 4H and 4I) was specifically and significantly increased in *dgit* mutants. These data indicate that dGIT is essential to ensure the efficacy of the slow phase of endocytosis and SV reacidification, which in our hands predominates postexocytosis processing ($Amp_{slow} > Amp_{fast}$). This provides a mechanistic explanation for the endocytic defects observed by EM and FM1-43 dye uptake experiments in the absence of dGIT.

Collectively, our results unravel a presynaptic role of GIT in SV recycling that is linked at least in part to its ability to regulate the expression level and localization of the synaptotagmin-specific endocytic sorting adaptor stonin 2/stoned B.

DISCUSSION

We have shown here that the CAZ-associated protein GIT physically and functionally associates with the endocytic adaptor stonin2/stoned B (Figure 1). Loss of function of dGIT in *Drosophila* leads to reduced levels of stoned B and its endocytic cargo synaptotagmin (Figure 2) and to endocytic defects (Figures 3 and 4), a phenotype that resembles that of *stoned* mutants. Presynaptic rescue experiments further demonstrate that the presynaptic role of GIT is independent of its established postsynaptic functions (Bahri et al., 2009; Zhang et al., 2005). These data, together with the localization of stonin at the periphery of AZs (Figure 1) and with the partitioning of stonin and several other endocytic proteins into detergent-resistant fractions containing CAZ proteins such as ELKS and GIT1 (Figure 1; Phillips et al., 2001), favor a hypothetical model in which GIT acts as a molecular bridge for the recruitment of stonin 2/stoned B to the periphery of the AZ. Physical connections between the AZ-based exocytic apparatus and the endocytic machinery may regulate vesicle reformation and thus availability, thereby contributing to efficient SV exo-endocytic cycling (Haucke et al., 2011; Hosoi et al., 2009; Sakaba et al., 2013; Xu et al., 2013). Our finding that *dgit* mutants show a selective defect in the slow component of SV recycling and reacidification (Figure 4) is explained best by a speculative model according to which exocytosed SV membranes are internalized via clathrin-dependent (Granseth et al., 2006) and clathrin-independent (Watanabe et al., 2013) pathways, the latter of which results in the formation of endosomal vacuoles from which SVs are regenerated. Loss of *dgit* in this model does not affect membrane retrieval per se, but selectively impairs slow, presumably clathrin- (Heerssen et al., 2008) and stoned B-mediated reformation of acidified SVs. We thus favor a hypothetical scenario in which the dGIT-stoned B complex in conjunction with other factors regulates SV reformation from internalized endosomal structures in order to replenish SVs close to the AZ (as recently observed at mammalian synapses; Schikorski, 2014). Further studies are required to put this model to the test. As GIT1 has been implicated in neuropsychiatric diseases such as ADHD (Won et al., 2011), the results reported here raise the possibility that GIT-dependent changes in presynaptic function may underlie ADHD-like disease in mice and men.

EXPERIMENTAL PROCEDURES

Confocal Microscopy of NMJs

Dissection, immunostaining, and confocal imaging of larval NMJs were done as described previously (Fouquet et al., 2009). Stacks from third instar larval muscle 4 (step size 0.5 μm) were acquired with a Leica TCS-SP5 microscope and a 63 × 1.4 NA oil objective (Leica) under the control of Application Suite Advanced Fluorescence (LAS-AF; Leica) software. ImageJ was used for maximum projections of stacks, quantification of areas, and fluorescence intensity profiles. To assess the distribution of endocytic proteins within boutons in Figures S2C and S2D, line scans were used to define the cortex of the bouton. Fluorescence intensities/area were measured for the bouton cortex versus the bouton lumen and set to one for WT larval NMJs.

Statistics

Data were analyzed by unpaired Student's t test or a one-way ANOVA using GraphPad. Data represent mean ± SEM, and n indicates the number of samples examined. Asterisks denote significance (n.s., $p > 0.05$; *$p < 0.05$; **$p < 0.001$; ***$p < 0.0001$).

For further information regarding the materials and methods used in this work, see Supplemental Experimental Procedures.

SUPPLEMENTAL INFORMATION

Supplemental Information includes Supplemental Experimental Procedures, four figures, and one table and can be found with this article online at http://dx.doi.org/10.1016/j.celrep.2014.04.051.

ACKNOWLEDGMENTS

We thank Drs. P.A. Randazzo (NIH), V. Hsu (Harvard Medical School), O. Shupliakov (Karolinska Institute), and N.E. Reist (Colorado State University) for reagents and Prof. S.W. Hell and F. Göttfert for help with STED microscopy. This work was supported by grants from the DFG (SFB958/A01 and HA2686/4-1 to V.H., SFB958/Z02 to J.S., and SFB958/A03 and SFB958/A06 to S.J.S.) and the Chinese funding agency NSFC (30930033 and 31110103907 to Y.Q.Z.).

Received: October 1, 2013
Revised: April 9, 2014
Accepted: April 23, 2014
Published: May 29, 2014

REFERENCES

Bahri, S.M., Choy, J.M., Manser, E., Lim, L., and Yang, X. (2009). The Drosophila homologue of Arf-GAP GIT1, dGIT, is required for proper muscle morphogenesis and guidance during embryogenesis. Dev. Biol. *325*, 15–23.

Bruckner, J.J., Gratz, S.J., Slind, J.K., Geske, R.R., Cummings, A.M., Galindo, S.E., Donohue, L.K., and O'Connor-Giles, K.M. (2012). Fife, a Drosophila Piccolo-RIM homolog, promotes active zone organization and neurotransmitter release. J. Neurosci. *32*, 17048–17058.

Claing, A., Perry, S.J., Achiriloaie, M., Walker, J.K., Albanesi, J.P., Lefkowitz, R.J., and Premont, R.T. (2000). Multiple endocytic pathways of G protein-coupled receptors delineated by GIT1 sensitivity. Proc. Natl. Acad. Sci. USA *97*, 1119–1124.

Dani, A., Huang, B., Bergan, J., Dulac, C., and Zhuang, X. (2010). Superresolution imaging of chemical synapses in the brain. Neuron *68*, 843–856.

Diril, M.K., Wienisch, M., Jung, N., Klingauf, J., and Haucke, V. (2006). Stonin 2 is an AP-2-dependent endocytic sorting adaptor for synaptotagmin internalization and recycling. Dev. Cell *10*, 233–244.

Dittman, J., and Ryan, T.A. (2009). Molecular circuitry of endocytosis at nerve terminals. Annu. Rev. Cell Dev. Biol. *25*, 133–160.

Fergestad, T., and Broadie, K. (2001). Interaction of stoned and synaptotagmin in synaptic vesicle endocytosis. J. Neurosci. *21*, 1218–1227.

Fouquet, W., Owald, D., Wichmann, C., Mertel, S., Depner, H., Dyba, M., Hallermann, S., Kittel, R.J., Eimer, S., and Sigrist, S.J. (2009). Maturation of active zone assembly by Drosophila Bruchpilot. J. Cell Biol. *186*, 129–145.

Göttfert, F., Wurm, C.A., Mueller, V., Berning, S., Cordes, V.C., Honigmann, A., and Hell, S.W. (2013). Coaligned dual-channel STED nanoscopy and molecular diffusion analysis at 20 nm resolution. Biophys. J. *105*, L01–L03.

Granseth, B., Odermatt, B., Royle, S.J., and Lagnado, L. (2006). Clathrin-mediated endocytosis is the dominant mechanism of vesicle retrieval at hippocampal synapses. Neuron *51*, 773–786.

Gundelfinger, E.D., and Fejtova, A. (2012). Molecular organization and plasticity of the cytomatrix at the active zone. Curr. Opin. Neurobiol. *22*, 423–430.

Haucke, V., Neher, E., and Sigrist, S.J. (2011). Protein scaffolds in the coupling of synaptic exocytosis and endocytosis. Nat. Rev. Neurosci. *12*, 127–138.

Heerssen, H., Fetter, R.D., and Davis, G.W. (2008). Clathrin dependence of synaptic-vesicle formation at the Drosophila neuromuscular junction. Curr. Biol. *18*, 401–409.

Hosoi, N., Holt, M., and Sakaba, T. (2009). Calcium dependence of exo- and endocytotic coupling at a glutamatergic synapse. Neuron *63*, 216–229.

Hua, Y., Sinha, R., Thiel, C.S., Schmidt, R., Hüve, J., Martens, H., Hell, S.W., Egner, A., and Klingauf, J. (2011). A readily retrievable pool of synaptic vesicles. Nat. Neurosci. *14*, 833–839.

Kaeser, P.S., Deng, L., Wang, Y., Dulubova, I., Liu, X., Rizo, J., and Südhof, T.C. (2011). RIM proteins tether Ca2+ channels to presynaptic active zones via a direct PDZ-domain interaction. Cell *144*, 282–295.

Kim, S., Ko, J., Shin, H., Lee, J.R., Lim, C., Han, J.H., Altrock, W.D., Garner, C.C., Gundelfinger, E.D., Premont, R.T., et al. (2003). The GIT family of proteins forms multimers and associates with the presynaptic cytomatrix protein Piccolo. J. Biol. Chem. *278*, 6291–6300.

Kittel, R.J., Wichmann, C., Rasse, T.M., Fouquet, W., Schmidt, M., Schmid, A., Wagh, D.A., Pawlu, C., Kellner, R.R., Willig, K.I., et al. (2006). Bruchpilot promotes active zone assembly, Ca2+ channel clustering, and vesicle release. Science *312*, 1051–1054.

Kononenko, N.L., Diril, M.K., Puchkov, D., Kintscher, M., Koo, S.J., Pfuhl, G., Winter, Y., Wienisch, M., Klingauf, J., Breustedt, J., et al. (2013). Compromised fidelity of endocytic synaptic vesicle protein sorting in the absence of stonin 2. Proc. Natl. Acad. Sci. USA *110*, E526–E535.

Koo, S.J., Markovic, S., Puchkov, D., Mahrenholz, C.C., Beceren-Braun, F., Maritzen, T., Dernedde, J., Volkmer, R., Oschkinat, H., and Haucke, V. (2011). SNARE motif-mediated sorting of synaptobrevin by the endocytic adaptors clathrin assembly lymphoid myeloid leukemia (CALM) and AP180 at synapses. Proc. Natl. Acad. Sci. USA *108*, 13540–13545.

Lampe, A., Haucke, V., Sigrist, S.J., Heilemann, M., and Schmoranzer, J. (2012). Multi-colour direct STORM with red emitting carbocyanines. Biol. Cell *104*, 229–237.

Liu, K.S., Siebert, M., Mertel, S., Knoche, E., Wegener, S., Wichmann, C., Matkovic, T., Muhammad, K., Depner, H., Mettke, C., et al. (2011). RIM-binding protein, a central part of the active zone, is essential for neurotransmitter release. Science *334*, 1565–1569.

Menon, P., Deane, R., Sagare, A., Lane, S.M., Zarcone, T.J., O'Dell, M.R., Yan, C., Zlokovic, B.V., and Berk, B.C. (2010). Impaired spine formation and learning in GPCR kinase 2 interacting protein-1 (GIT1) knockout mice. Brain Res. *1317*, 218–226.

Miesenböck, G., De Angelis, D.A., and Rothman, J.E. (1998). Visualizing secretion and synaptic transmission with pH-sensitive green fluorescent proteins. Nature *394*, 192–195.

Miśkiewicz, K., Jose, L.E., Bento-Abreu, A., Fislage, M., Taes, I., Kasprowicz, J., Swerts, J., Sigrist, S., Versées, W., Robberecht, W., and Verstreken, P. (2011). ELP3 controls active zone morphology by acetylating the ELKS family member Bruchpilot. Neuron *72*, 776–788.

Mullen, G.P., Grundahl, K.M., Gu, M., Watanabe, S., Hobson, R.J., Crowell, J.A., McManus, J.R., Mathews, E.A., Jorgensen, E.M., and Rand, J.B. (2012). UNC-41/stonin functions with AP2 to recycle synaptic vesicles in Caenorhabditis elegans. PLoS ONE *7*, e40095.

Owald, D., Fouquet, W., Schmidt, M., Wichmann, C., Mertel, S., Depner, H., Christiansen, F., Zube, C., Quentin, C., Körner, J., et al. (2010). A Syd-1 homologue regulates pre- and postsynaptic maturation in Drosophila. J. Cell Biol. *188*, 565–579.

Phillips, G.R., Huang, J.K., Wang, Y., Tanaka, H., Shapiro, L., Zhang, W., Shan, W.S., Arndt, K., Frank, M., Gordon, R.E., et al. (2001). The presynaptic particle web: ultrastructure, composition, dissolution, and reconstitution. Neuron *32*, 63–77.

Sakaba, T., Kononenko, N.L., Bacetic, J., Pechstein, A., Schmoranzer, J., Yao, L., Barth, H., Shupliakov, O., Kobler, O., Aktories, K., and Haucke, V. (2013). Fast neurotransmitter release regulated by the endocytic scaffold intersectin. Proc. Natl. Acad. Sci. USA *110*, 8266–8271.

Schikorski, T. (2014). Readily releasable vesicles recycle at the active zone of hippocampal synapses. Proc. Natl. Acad. Sci. USA *111*, 5415–5420.

Segura, I., Essmann, C.L., Weinges, S., and Acker-Palmer, A. (2007). Grb4 and GIT1 transduce ephrinB reverse signals modulating spine morphogenesis and synapse formation. Nat. Neurosci. *10*, 301–310.

Stimson, D.T., Estes, P.S., Rao, S., Krishnan, K.S., Kelly, L.E., and Ramaswami, M. (2001). Drosophila stoned proteins regulate the rate and fidelity of synaptic vesicle internalization. J. Neurosci. *21*, 3034–3044.

Verstreken, P., Ohyama, T., and Bellen, H.J. (2008). FM 1-43 labeling of synaptic vesicle pools at the Drosophila neuromuscular junction. Methods Mol. Biol. *440*, 349–369.

Watanabe, S., Rost, B.R., Camacho-Pérez, M., Davis, M.W., Söhl-Kielczynski, B., Rosenmund, C., and Jorgensen, E.M. (2013). Ultrafast endocytosis at mouse hippocampal synapses. Nature *504*, 242–247.

Won, H., Mah, W., Kim, E., Kim, J.W., Hahm, E.K., Kim, M.H., Cho, S., Kim, J., Jang, H., Cho, S.C., et al. (2011). GIT1 is associated with ADHD in humans and ADHD-like behaviors in mice. Nat. Med. *17*, 566–572.

Xu, J., Luo, F., Zhang, Z., Xue, L., Wu, X.S., Chiang, H.C., Shin, W., and Wu, L.G. (2013). SNARE proteins synaptobrevin, SNAP-25, and syntaxin are involved in rapid and slow endocytosis at synapses. Cell Rep *3*, 1414–1421.

Zhang, H., Webb, D.J., Asmussen, H., Niu, S., and Horwitz, A.F. (2005). A GIT1/PIX/Rac/PAK signaling module regulates spine morphogenesis and synapse formation through MLC. J. Neurosci. *25*, 3379–3388.

Cell Reports, Volume *7*

Supplemental Information

A Presynaptic Role for the Cytomatrix Protein GIT in Synaptic Vesicle Recycling

Jasmin Podufall, Rui Tian, Elena Knoche, Dmytro Puchkov, Alexander M. Walter, Stefanie Rosa, Christine Quentin, Anela Vukoja, Nadja Jung, Andre Lampe, Carolin Wichmann, Mathias Böhme, Harald Depner, Yong Q. Zhang, Jan Schmoranzer, Stephan J. Sigrist, and Volker Haucke

Supplementary Figures

Supplementary figure S1, related to figure 1

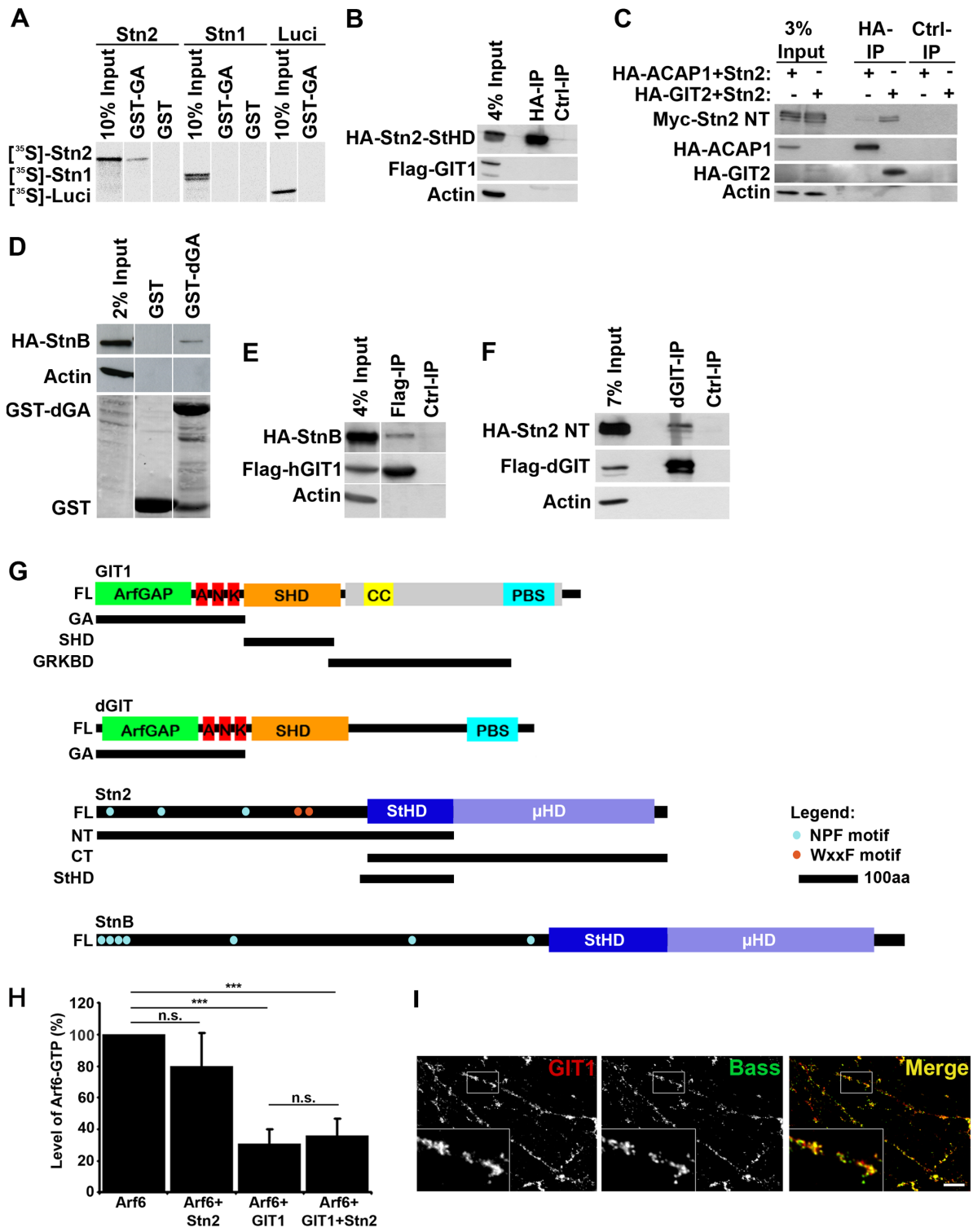

Supplementary figure S1 (related to fig. 1): GIT directly associates with Stonin.

(A) GIT1 does not interact with Stonin1 (Stn1), the closest homologue of Stn2. GIT1-GA pulled down *in vitro*-translated Stn2 but not Stn1 or Luciferase (Lucif) that was used as a

control. **(B)** Stn2 does not interact via its Stonin-homology domain (StHD) with GIT1. Flag-GIT1 was not co-immunoprecipitated with HA-Stn2-StHD from Cos7 cells transiently overexpressing both constructs. **(C)** Association of Stonin 2 with HA-GIT2 but not with ACAP1. Cells transiently overexpressing the N-terminal domain of Stonin 2 (Myc-Stn2-NT) together with HA-tagged GIT2 or ACAP1 were subjected to co-immunoprecipitation experiments using anti-myc antibodies. Samples were analyzed by immunoblotting with the indicated antibodies. **(D)** The ArfGAP domain of *D.mel* GIT binds to *D.mel* StnB. StnB was affinity-purified from extracts of cells transfected with HA-StnB using GST-GA of *D.mel* dGIT (dGA) or GST as a control. (**E, F)** The interaction sites of the GIT-Stonin-complex are conserved between mammals and D.*mel*. Fly StnB-HA co-immunoprecipitated with human Flag-GIT1 (**E**) and human HA-Stn2 NT interacted with fly Flag-dGIT (**F**) in transfected Cos7 cells. **(G)** Scheme of full length and truncation mutants of GIT1, dGIT, Stn2 and StnB used in this study. **(H)** Stonin 2 does not regulate the ArfGAP activity of GIT1. Cells stably expressing Stn2 were co-transfected with HA-Arf6 and FLAG-GIT1. 24h post-transfection expression of Stn2 was induced by addition of doxycycline. 24h later, Arf6-GTP was affinity-purified from these TX100-cell extracts (supplemented with 100µM GTP and GDP) using GST-GGA3-VHS/GAT. Arf6-GDP (T44N) was used as a negative control. GST-precipitates were analyzed by SDS-PAGE and immunoblotting. The levels of GTP Arf6-HA were quantified by anti-HA-antibodies detected with ^{125}-I protein A and phosphoimage analysis. The levels of Arf6-GTP do not significantly change upon Stn2 overexpression (control=Arf6 only: 100; Arf6+Stn2: 77.9±19.6, p=0.358 to control, n.s.). Arf6-GTP levels are significantly reduced by overexpressing GIT1 (Arf6+GIT1: 31.6±8.6, p<0.0001 to control, ***). This effect remains unchanged by co-transfection of Stn2 with GIT1 (Arf6+GIT1+Stn2: 25.5±9.6, p<0.0001 to control, ***; p=0.713 to Arf6+GIT1, n.s.). n=7 experiments. Student`s t-test. Data represent mean ± SEM. **(I)** GIT1 partially co-localizes with the AZ protein Bassoon in rat hippocampal neurons (DIV14). Scale bar, 10µm.

Supplementary figure S2, related to figure 2

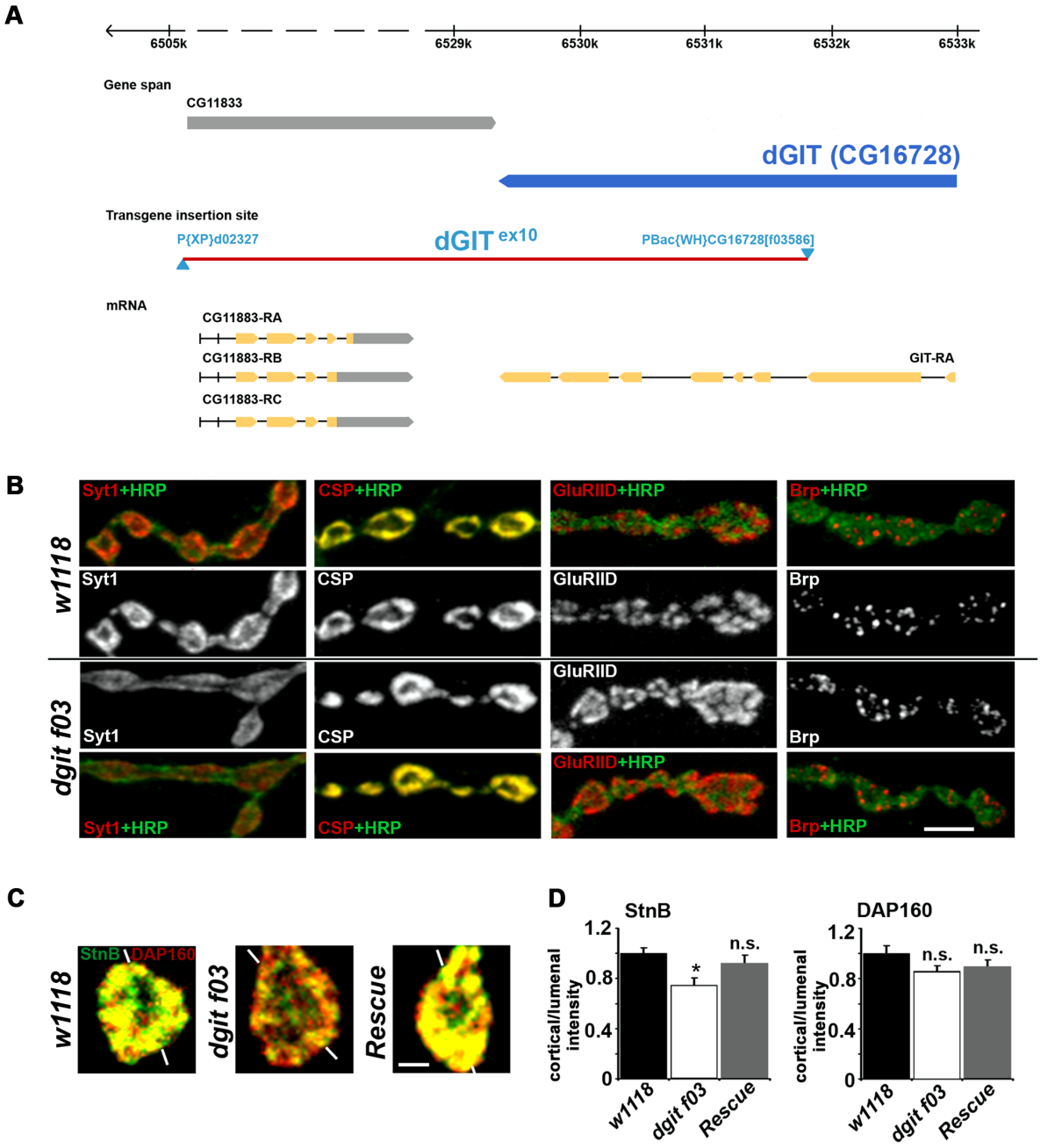

Supplementary figure S2 (related to fig. 2): dGIT regulates presynaptic levels and localization of stoned B and synaptotagmin 1 at *Drosophila* NMJ synapses

(A) Schematic overview of the dGIT genomic region and the *dgit* mutants used in this study. The excision mutant *dgitex10* (red dash) resulting in a complete deletion of the SHD and PBS domains was produced based on FLP-FRT recombination between the *dgitf03586* (PBac{WH}*gitf03586*) and *CG11883d02327* transposon lines. The excision mutant was

crossed with *dgitf03586* (piccybac transposon PBac{WH}*gitf03586*) yielding *dgitf03586/10* (termed *dgit f03*) used throughout the study. Yellow boxes represent *dgit* exons (lower panel). Modified from www.flybase.org. **(B)** Wild-type (**(**w^{1118}), dGIT mutant (*dgit f03*) and *dgit rescue* larvae were stained with different markers as indicated. Representative images used for quantifications shown in figure 2G-J are shown. Levels of synaptotagmin 1 (Syt1) are reduced in *dgit* mutants. By contrast, the levels of CSP remain unchanged. Postsynaptic glutamate receptor (GluRIID) levels are increased, likely as a result of compensation. **(C-D)** StnB is mislocalized in boutons from *dgit* mutant larvae. (**C)** Representative images of boutons stained for endogenous StnB (green) and Dap160/ intersectin (red) illustrating the partial redistribution of StnB from cortical areas towards the lumen of the bouton in *dgit* mutants (*dgit f03*). This is rescued by presynaptic re-expression of dGIT (*rescue*). The localization of Dap160/ intersectin is unaffected. White lines indicate line scans of fluorescence intensities along the longest axis of the boutons. Scale bar, 1µm. (**D)** Quantification of data shown in C for StnB (w^{1118}: 1.0±0.04, n=15; *dgit f03*: 0.75±0.06, n=17, p=0.0022; *rescue*: 0.92±0.07, n=15, p=0.322) and Dap160/intersectin (w^{1118}: 1.0±0.06, n=15; *dgit f03*: 0.86±0.04, n=17, p=0.063; *rescue*: 0.90±0.05, n=15, p=0.214). Data represent mean ± SEM. Student´s t-test.

Supplementary figure S3, related to figure 3

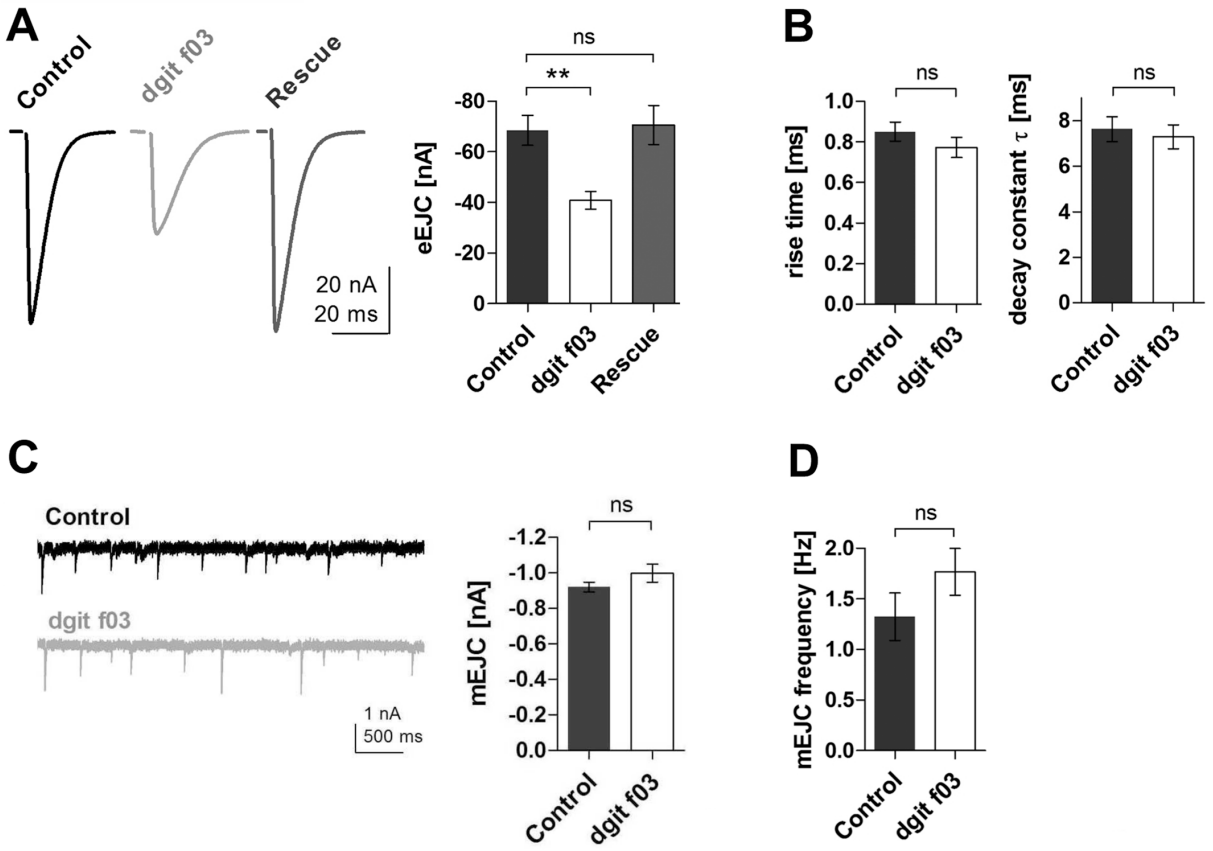

Supplementary figure S3 (related to fig. 3): Lack of dGIT impairs neurotransmission

(A) Example traces of eEJCs at 0.2 Hz nerve stimulation (left) and mean eEJC amplitudes (right) of control, *git f03* mutant and *rescue* larval NMJs (recorded in 1 mM extracellular Ca^{2+}). eEJC amplitudes are decreased in *git f03* mutants. (control: -68.5 ± 5.9 nA, n = 13*; git f03*: -40.8 ± 3.5 nA, n = 11; $p \leq 0.01$; one way ANOVA Tukey's post test). One copy of the genomic transgene restored evoked responses (rescue: -70.5 ± 7.7 nA, n = 10). **(B)** Rise time of eEJCs and decay constant τ are unaltered in *git f03* mutants compared to controls. (rise time; control: 0.85 ± 0.05 ms, n = 13; *git f03*: 0.78 ± 0.05 ms, n = 11; p = 0.31; students t-test; τ ; control: 7.6 ± 0.5 ms, n = 13; *git f03*: 7.3 ± 0.5 ms, n = 11; p = 0.77; students t-test). **(C)** (Left) Example traces of mEJCs. (Right) The mean mEJC amplitude is not significantly altered in *git f03* mutants (control: - 0.92 ± 0.03 nA, n = 11; *git f03*: -1.00 ± 0.05, n = 8; p = 0.23; students t-test). **(D)** mEJC frequency is insignificantly increased in *git f03* mutants (control: 1.32 ± 0.23, n = 11; *git f03*: 1.77 ± 0.23, n = 10; p = 0.19; students t-test). **(E)** (Left)

Example traces of paired-pulse stimulation for control (black) and *git f03* (grey) illustrate facilitation at *git f03* NMJs. (Right) PPR is significantly increased at *git f03* NMJs at 10 ms interstimulus interval (control: 1.03 ± 0.05, n= 15; *git f03*: 1.37 ± 0.11, n = 11; $p < 0.01$).

Supplementary figure S4 (related to figure 4)

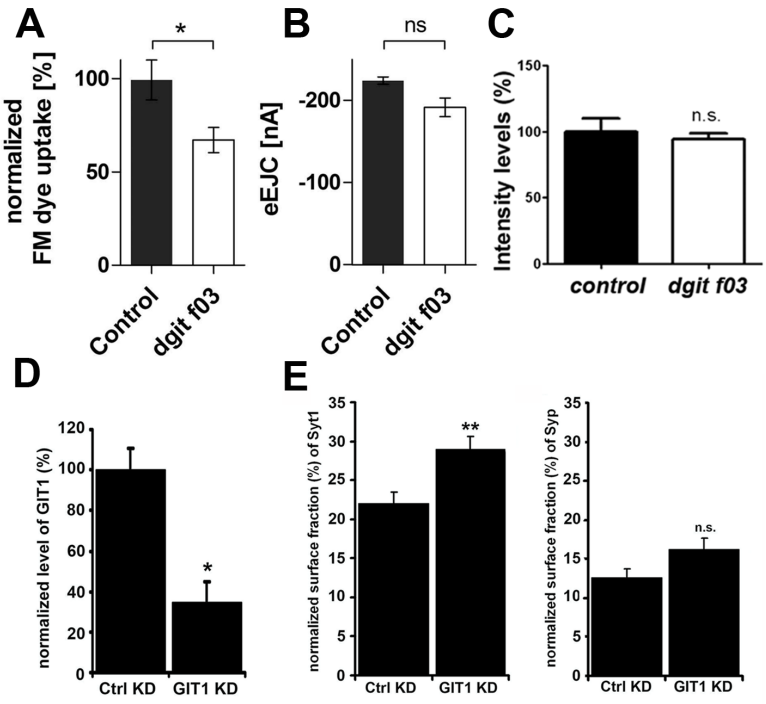

Supplementary figure S4 (related to fig. 4): Lack of GIT impairs SV recycling

(A) Elevated extracellular Ca^{2+} (5 mM) rescues defects in neurotransmitter release in *dgit f03* mutants. eEJC amplitudes are not significantly different between controls and *dgit f03* mutants (control: -224.0 ± 4.6 nA, n = 9*; git f03*: -191.6 ± 11.3 nA, n = 9; p > 0.05; students t-test).

(B) Elevated extracellular Ca^{2+} (5 mM) does not rescue endocytic defects in *dgit f03* mutants. Quantification of FM 1–43 dye labeling intensity after incubation of 3rd instar larval NMJs in 4 µM FM1-43 and stimulation for 5 min with 90 mM KCl, 5 mM $CaCl_2$. Data represent mean ± SEM, from at least 13 NMJs. (Student's *t* test, **P*< 0.05).

(C) Total synapto-pHluorin (SpH) expression levels in control (*OK6*; *UAS-SpH*) and *dgit f03* (*fo3/ex10,OK6*; *UAS-SpH*) synapses determined from quantitative imaging of NH_4Cl dequenched preparations.

(D, E) GIT1 regulates endocytic sorting of synaptotagmin in hippocampal neurons. **(D)** Efficient siRNA-mediated depletion of GIT1 in rat hippocampal neurons. Ctrl KD: 100 ±

10.4; GIT1 KD: 35.8 ± 10.7, n = 3 experiments; p = 0.0126; data represent mean ± SEM, *p < 0.05, Student´s t-test. **(E)** pHluorin-based measurement of surface vs. vesicular pools of SV proteins. Rat hippocampal neurons were cotransfected with pHluorin-tagged synaptotagmin 1 or synaptophysin together with GIT1-directed (GIT1 KD) or control siRNA (control KD). Synaptotagmin 1-pHluorin was partially redistributed to the surface of GIT1-depleted neurons (control KD: 22.1 ± 1.4; n = 16 neurons; GIT1 KD: 29.0 ± 1.6; n = 16 neurons; *p = 0.0027 to control) whereas effects on synaptophysin-pHluorin were statistically insignificant (control KD: 12.7 ± 1.1; n = 18 neurons; GIT1 KD: 16.2 ± 1.5; n = 15 neurons; p = 0.0557 to control, n.s.). Data represent mean ± SEM, n.s. p > 0.05; **p < 0.01; Student´s t-test.

Supplementary Table 1

	w^{1118} (wild-type)	***dgit f03***	***dgit f03-rescue***
Number of SVs per bouton area, #/µm²	147.72 ± 12.17	152.26 ± 18.16	150.08 ± 9.53
Number of endosomes per bouton area, #/µm²	1.79 ± 0.25	3.1 ± 0.39**	2.32 ± 0.55
Area of endosomes per bouton area, µm²/µm²	0.0206 ± 0.0045	0.0392 ± 0.0081*	0.0232 ± 0.0053
Active zone size, µm	0.491 ± 0.42	0.493 ± 0.037	0.447 ± 0.029
Number of T-bars per active zone length, #/µm	0.684 ± 0.205	0.922 ± 0.263	0.756 ± 0.222
Number of docked SVs per active zone	4.067 ± 0.411	4.07 ± 0.431	3.766 ± 0.33
Number of docked SVs per active zone length, #/µm	8.59 ± 0.72	8.48 ± 0.84	8.48 ± 0.57

* p≤0,04, ** p≤0.004

Supplementary experimental procedures

Plasmids

The following constructs were cloned into pGEX4T-1 (Amersham Biosciences) for bacterial expression: full-length (FL, aa1-761) or truncation mutants (GA, aa1-254; SHD, aa251-374; GRKBD, aa363-645) of human GIT1; full-length (aa1-731) or GA domain of *D. melanogaster* GIT (dGA, aa1-304, derived from Flybase #LD30319); human GGA3-VHS/GAT (aa1-313, a kindgift from Dr. P.A. Randazzo, NIH; Bethesda, MD). dGIT aa590-731 and StnB aa48-148 werecloned into pet28a+ (Novagen) for bacterial expression. The following constructs were cloned into custom made vectors based on pcDNA3 (Invitrogen) for N-terminally HA-, Myc- or Flag-tagged protein expression in mammalian cells: human Stn2 constructs (FL, aa1-898; NT, aa1-555; CT, aa421-898; StHD, aa414-555); mouse Stonin1 (aa1-817, derived from RIKEN #6030478E24); human HA-GIT2 (aa1-471, PCR from ImageGenes #IRAUp969G046D6); human HA-ACAP1 (derived from pcDNA3.1 Myc-His-ACAP1, a kind gift from Dr. V. Hsu, Harvard Medical School); human Flag-tagged constructs of GIT1 FL (aa1-761) or its GA domain (aa1-254); human HA-Arf6 wildtype and HA-Arf6 T44N; D.*mel* HA-StnB FL (aa1-1262, derived from DGRC #RH38069) and D.*mel* Flag-dGIT FL (aa1-731; derived from DGRC #LD30319). Superecliptic pHluorin tagged synaptotagmin 1 was generated as previously described (Wienisch and Klingauf, 2006). Synaptophysin fused to pHluorin is a kind gift from Dr. Lagnado. Full-lenth (aa1-731) as well as ΔGA dGIT (aa 304-731, both derived from DGRC #LD30319) were cloned into the entry plasmid pENTR4. pUASt-*dGIT* cDNA, pTW-*dGIT* cDNA, and pTGW-*dGIT* cDNA (for N-terminal GFP-tag) were generated from entry plasmids using the GATEWAY system (Invitrogen). All constructs were verified by DNA sequencing (MWG).

Oligonucleotides

The following published siRNAs were used: rat GIT1 siRNA (Zhang et al., 2005) and control siRNA (Bushlin et al., 2008). The following primer pairs were used for genotyping Stonin2 KO mice by PCR of genomic DNA obtained from tail biopsies: 5'GATCCCCGGGGCCCCCTCACCTGCCTCA3' and 5'GATCCTCGAGCTAGGACAGCACTGGTAAATCCA3' (for WT) and 5'GGCGCGGTCCCAGGTCCAC3' and 5'CTTCGCCCAATAGCAGCCAGTCC3' (for KO allele).

Antibodies

The following mouse monoclonal antibodies were used: HA (HA.11, Babco/Convance), FLAG (M2, Sigma), Actin (AC-15, Sigma), clathrin heavy chain (TD.1, own stocks), a-adaptin (AP6, homebrew), Tubulin (B512, Sigma), Bassoon (219E1, Synaptic Systems), Synaptophysin (7.2, Synaptic Systems), Synaptotagmin1 (41.1, Synaptic Systems), GRIP (#611318, BD Bioscience), ELKS (ab50312, Abcam), Dynamin (#610245, BD Bioscience), c-myc (9E10, own stocks), CSP (6D6, DSHB), Brp (Nc82, DSHB). The following rabbit polyclonal antibodies were used: GIT1 (H170, Santa Cruz), Stonin 2 [2423.4, own stocks (Walther et al., 2004)], GFP (ab6556, Abcam for cell culture or A11122, Invitrogen), Picollo (#142002, Synaptic Systems), Synapotagmin1 (CL1, a kind gift from Dr. N. Reist) and GluR2D (Qin et al., 2005). Additionally, chicken polyclonal GFP (ab13970, Abcam), guinea pig polyclonal Dap160 (a kind gift from Dr. O. Shupliakov, Karolinska Institute) and goat HRP-Cy5 (Dianova) antibodies were used for *D. melanogaster* stainings. Polyclonal antibodies against dGIT and StnB were raised in rabbits by injecting of His6-dGIT (aa590-731) or His6-StnB (aa48-148), respectively. The sera were tested for specificity and affinity purified. Following 2nd antibodies were used: AlexaFluor^{488}, AlexaFluor^{568}, AlexaFluor^{647} and AlexaFluor^{700} (Molecular Probes), Chromeo^{494} and Atto^{647N} (Active Motif) and HRP-coupled 2nd antibodies for immnuoblot development (Dianova).

Generation of dGIT Mutants and Transgenic Flies

Fly strains were reared under standard laboratory conditions (Sigrist et al., 2003) at 25 °C on a semi-defined medium (Bloomington recipe). Mutants used in this study were: The excision mutant *dgit*ex10, which partially deletes the *dgit* as well as the neighboring 5' *StIP* locus, was produced based on FLP-FRT recombination (Parks et al., 2004) between the *dgit*f03586 (PBac{WH}*git* f03586) and *CG11883 d02327* transposon lines. The excision mutant was crossed with Df(2R)Df596 or *dgit*f03586 (piccybac transposon of *dgit* gene PBac{WH}*git* f03586) yielding *dgit*Df596/*dgit*ex10 ("dgitex10/Df") or *dgit*f03586/ *dgit*ex10 ("dgitf03"), respectively. Transgenic animals (BestGene, Inc.) were established in the *w1118* background. The following genotypes were used: a) *w1118/ok6-GAL4* as control, b) *dgit*f03586*/dgit*ex10,*ok6-GAL4* as *dgit f03; c) dgit*Df596*/dgit*ex10,*ok6-GAL4* as *dgit Df*; *d) dgit*f03586*/dgit*ex10*,ok6-GAL4;* UAS-*dGIT*/+ as *f03 rescue; e) dgit*Df596*/dgit*ex10,*ok6-GAL4;*UAS-*dGIT*/+ as *Df rescue ; f)* UAS-GFPdGIT cDNA/*ok6-GAL4 as* dGITGFP. Genotypes used for locomotion tests and immunoblottings were a) *w1118/elav^{c155}-GAL4;* b) *elav^{c155}-GAL4*/Y; *dgit*f03586*/dgit*ex10 as *dgit f03;* c) *elav^{c155}-GAL4*/Y; *dgit*f03586*/dgit*ex10*;* UAS-*dGIT*cDNA/+ as *f03 rescue*; d) *elav^{c155}-GAL4*/Y;*dgit*f03586*/dgit*ex10*;*UAS-GFP-*dGIT*cDNA/+ as *f03 dgit-GFP rescue*; e) *elav^{c155}-GAL4*/Y;*dgit*Df59*6/dgit*ex10 *as dgit Df.*

For SpH imaging the synapto-pHluorin transgene UAS-SpH was expressed presynaptically using OK6-GAL4 driver in all synaptopHluorin experiments.

Locomotion

Tests with individual flies were done as previously described (Owald et al., 2010). In short, wings of flies were clipped prior to testing. For negative geotaxis, flies were placed in an empty food vial and their maximum height reached within 30 s was measured. All tests were done under red light.

CAZ Preparation

Purification of presynaptic cytomatrix at the active zone (CAZ) was done as described previously (Phillips et al., 2001). Equal amounts of soluble (sup) and insoluble material (pellet) were analyzed by SDS/PAGE and immunoblotting.

Cell Culture and Transfections

Cos7, HEK293 and HEK293 FlipIn cells stably transfected with HA-Stn2 were grown in Dulbecco's modified Eagle's medium (Invitrogen) supplemented with fetal calf serum and antibiotics. Protein expression in stably transfected cell lines was induced by addition of 1µg/ml Doxycyclin. Cells were transfected using Lipofectamine2000 Reagent (Invitrogen).

Recombinant Protein Purification and GST-Pulldown

GST- or His_6-fusion proteins were expressed in E.*coli* BL21 (DE3). Proteins were purified using standard protocols. For GST-pulldowns, immobilized GST-fusion proteins (50-100 µg) were incubated in assay buffer [20 mM HEPES (pH 7.4), 100 mM KCl, 2 mM MgCl2, 1% Triton X-100)] for 2 h at 4 °C with precleared Triton X-100–lyzed cell extracts (1mg/ml) supplemented with 1 mM PMSF and protease inhibitor mixture (Sigma). Proteins were washed, eluted with sample buffer and analyzed by SDS/PAGE and immunoblotting.

Immunoprecipitation from Rat Brain and Fly Head Extracts

Rat brains were homogenized in 4 mM HEPES (pH 7.4), 320 mM sucrose, 1 mM PMSF and protease inhibitor mixture (Sigma). Homogenates were centrifuged at 1,000 x g for 10 min. Supernatants were adjusted to 20 mM HEPES pH 7.4, 100 mM KCl, 2 mM $MgCl_2$ and 1% Triton X-100 (assay buffer) and incubated on ice for 10min. The extracts were centrifuged for 15 min at 40,000 x g and 4 °C before ultra-centrifugation (15min, 4 °C, 180,000 x g). The

resulting supernatant was used for immunoprecipitation (IP) experiments (1-2mg extract) or large scale IPs (35mg extract, see below). Fly heads used for IPs were homogenized in assay buffer supplemented with 1 mM PMSF. Homogenates were ultracentrifuged (170,000 x g, 15min, 4 °C). The proteinaceous phase was recovered after washing by a second ultracentrifugation step and used for IPs (1-2mg extract). For IPs, extracts were incubated with antibodies immobilized on Protein A/G PLUS-Agarose beads (Santa Cruz) in assay buffer at 4°C for 2h. Bound proteins were washed, eluted with sample buffer and analyzed by SDS/PAGE, Coomassie blue staining and immunoblotting. For large scale IPs, purified anti-Stn2 IgGs (or pre-immune IgGs as controls) immobilized on CNBr-activated SepharoseTM 4B (GE Healthcare) were used. Potential stonin 2 interacting proteins were excised from colloidal Coomassie-stained SDS PAGE gels and subjected to mass spectrometry for identification (Dr. Chris Weise, FU Berlin). GIT1 was identified as a stonin 2 binding partner in two independent experiments.

Direct Protein Binding Assay

GST-fusion proteins were expressed and purified as mentioned before. Stn2-HA, Stn1-HA and Luciferase (as negative control) were expressed as radioactively-[^{35}S]-labeled proteins from plasmid DNA using the TNT Coupled Reticulocyte Lysate kit (Promega). In brief, 0.5 µg DNA was incubated with RNA polymerase, the amino acid mixture without methionine and [^{35}S]-methionine for radiolabeling of proteins for 90min at 30 °C. Immobilized GST-fusion proteins (2 µg) were incubated with 10 µl of precleared radiolabeled proteins in 0.1 ml assay buffer [20 mM HEPES (pH 7.4), 150 mM NaCl, 2 mM $_{MgCl2}$, 320 mM sucrose, 1 mM DTT, 1% CHAPS)] for 90min at 4 °C. Proteins were washed, eluted with sample buffer and analyzed by SDS/PAGE and Coomassie-staining. Radioactive proteins were visualized using PhosphorImage films (Cyclone Systems, Packard) and quantified (OptiQuant Software, Packard).

Arf6-GTP Assay

HekFlipIn cells with inducible expression of Stn2 were transfected with HA-Arf6 wt (or HA-Arf6 T44N as control) and Flag-GIT1. 24h later, Stonin 2 expression was induced by adding Doxycycline. After an additional 24h, HA-Arf6-GTP was affinity-purified from Triton X-100-cell extracts (supplemented with 100µM GTP and GDP) using GST-GGA3-VHS/GAT as described for IPs. GST-precipitates were analyzed by SDS/PAGE and immunoblot. The levels of GTP Arf6-HA were quantified using an anti-HA-antibody, subsequent incubation with ^{125}-I Protein A and analysis with Phosphor Imager (Packard) and OptiQuant software (Packard).

FM Dye Uptake

For FM1-43 uptake into vesicles in nerve terminals during reformation after depletion (Kuromi et al., 1997; Ramaswami et al., 1994) the Sylgard dish with the preparation was placed in a 34 °C incubation chamber and the medium was replaced by prewarmed normal medium (34 °C). After allowing 5 min for the temperature to equilibrate, the preparation was stimulated with high K+ saline for 5 min at 34 °C to deplete vesicles in the nerve terminals. The preparation was then removed from the 34 °C incubation chambers, and the medium replaced with medium containing 4 µM FM1-43 at 34°C and incubated for 5 min. The preparations were finally washed in Ca^{2+}-free saline (3x, 5min total time). The composition of the extracellular haemolymph-like saline (HL-3) (Verstreken et al., 2008) was (in mM): NaCl 110, KCl 5, $MgCl_2$ 10, $NaHCO_3$ 10, trehalose 5, sucrose 30, HEPES 5, pH 7.2. When stimulated with 90 mM K+, preparations were incubated in a modified HL-3 with reduced NaCl to preserve osmolarity. $CaCl_2$ was added to obtain a final concentration of 1.5 mM or 5mM depending on the experiment. Single optical slices from boutons on muscle 4, segment A2 and A3 were acquired using a 40X water immersion lens and a upright epifluorescence Olympus BX51WI microscope equipped with a Hamamatsu Orca ER cooled CCD digital

camera and a Visitron Lambda DG-4 illumination system. Images were processed in ImageJ software and the statistical analysis performed with GraphPad Prism 5 software.

Immunofluorescence Microscopy of Hippocampal Neurons

Hippocampal neurons from neonatal Wistar rat brain (P1-P3) were transfected on 9-11 day *in vitro* (DIV) by a modified calcium phosphate (Promega) procedure. Neurons (DIV13-16) were fixed with 4% PFA, 4% sucrose in PBS for 20min at RT or with ice-cold methanol for 7 min at -20°C (for AP2). Cells were washed, blocked (30% goat serum and 0.3% Triton X-100 in PBS) and incubated with 1^{st} antibodies in block solution (1 h at RT). After washing, cells were incubated with fluorescently labeled 2^{nd} antibodies in block solution (1 h, RT). Cells were washed with PBS and mounted on glass slides with Immumount Solution (Thermo Scientific). Image aquisition was performed using an inverted epifluorescence microscope (Zeiss) or a spinning disc confocal microscope (Perkin Elmer).

SD-dSTORM

Spectral demixing *direct* stochastic optical reconstruction microscopy (SD-*d*STORM) was used for simultaneous dual-color imaging of single molecules according to (Lampe et al., 2011). Neurons were prepared, transfected and immunostained (using AlexaFluor^{647} and AlexaFluor^{700} as 2^{nd} antibodies) as described for confocal imaging. Neurons were imaged at the custom-built SD-*d*STORM setup with a 100x oil objective (Nikon, APO 100x 1.49 NA) and a 1.5 magnification lens controlled by MicroManager (UCSF) and ImageJ (NIH). Both red fluorophores were illuminated with 643nm to switch them into the OFF state. After blinking of individual molecules started, we acquired (with 405nm irradiation at <1W/cm^2) a sequence of 20,000 frames at an exposure time of 30ms. The emission light was split via OptoSplit II (Cairn Optics), a dichroic mirror (710 DXCR) and emission filters (HC687/40 and ET794/160) into a short and a long wavelength channel, i.e. two sides of the field of view.

Localization of single molecules was identified with the open source software rapidSTORM 1.4.9 (Wolter et al., 2010). A custom-written algorithm (Lampe et al., 2011) was used to 1) identify localization pairs based on their geometric position in both channels/both sides of field of view, 2) to assign colors via plotting localization pairs intensities in a 2D histogram and 3) to finally reconstruct a dual-color image (pixel size: 17.3nm) by plotting the color assigned localizations.

2-color STED microscopy of Drosophila larval NMJs

Primary antibodies were used in the following concentrations: mouse monoclonal antibody 3E6 = anti-GFP 1:500 (Invitrogen), rabbit anti-dsRed 1:500 (Clontech). Secondary antibodies for STED were used in the following concentrations: goat anti-mouse Atto590 1:100 and goat anti-rabbit star635 1:100 (Atto590 (ATTO-TEC) and star635 (Abberior) coupled to respective IgGs (Dianova)). For STED imaging larvae were mounted in Mowiol. Images from fixed samples were taken from 3rd instar larval NMJs. 2-color STED images were recorded on a custom-built STED-microscope (Göttfert et al., 2013), which combines two pairs of excitation laser beams of 595 nm and 640 nm wavelength with one STED fiber laser beam at 775 nm. STED images were processed using a linear deconvolution function integrated into Imspector Software (Max Planck Innovation GmbH). The point spread function (PSF) for deconvolution was generated by using a 2D Lorentz function with its FWHM fitted to resolution estimate of each individual image. Images for figures were processed with ImageJ software to remove background.

Structured illumination microscopy (SIM) of Drosophila larval NMJs

Structured Illumination Microscopy (SIM) was done on the OMX V4 Blaze from Applied Precision Instruments (GE Healthcare). We used the 488nm (dGit-GFP) and 568nm (Stoned

B) channels with z-slices of 125nm thickness. The SIM image in figure 1J is a maximum projection of three consecutive z-slices in the center of the NMJ bouton.

Electrophysiology

TEVC recordings were performed at room temperature (RT) on male, 3rd instar, larval NMJs (muscle 6, segments A2, A3) essentially as previously reported (Kittel et al., 2006). The composition of the extracellular haemolymph-like saline (HL-3) (Stewart et al., 1994) was (in mM): NaCl 70, KCl 5, $MgCl_2$ 20, $NaHCO_3$ 10, trehalose 5, sucrose 115, HEPES 5, $CaCl_2$ 1, pH adjusted to 7.2. For recordings in elevated Ca^{2+} (5 mM) MgCl was reduced to 10 mM. Recordings were made from cells with an initial Vm between –40 and –60 mV, and input resistances of ≥ 4 MΩ, using intracellular electrodes with resistances of 8-20 MΩ, filled with 3 M KCl. Both eEJCs, which reflect the compound EJC of both motoneurons innervating muscle 6, (voltage clamp at -60 mV) and mEJCs (voltage clamp at -80 mV) were low-pass filtered at 1 kHz. Miniature EJC recordings lasted for 90 s. Paired-pulse recordings consisted of 10 traces/ interval/ cell, 4 s rest were left between the two pulses. The amplitude of the 2nd pulse in 10 ms ISI paired-pulse recordings was measured from the peak to the point of interception with the extrapolated 1st pulse. 0.2 Hz stimulation protocols included at least 10 traces/ cell. The rise time and decay time constant (τ) were obtained from the average event of the corresponding recording. The rise time was measured from 10 to 90 % of the maximum amplitude, and the decay was fit with a single exponential function from 60 % of the peak. Highfrequency stimulation followed 30 s rest. Controls were either w1118 or carried one copy of *ok6*-GAL4. The recordings were analyzed with pClamp 10 (Molecular Devices, Sunnyvale, CA, USA) and MATLAB R2010b (Mathworks, Natick, MA, USA). Stimulation artifacts of eEJCs were removed for clarity. The data are reported as mean ± SEM unless otherwise noted; n indicates the number of cells examined.

Electron Microscopy

Drosophila 3rd instar larvae fillets were prepared in calcium-free HL-3 [(in mM): NaCl 110, KCl 5, $MgCl_2$ 10, $NaHCO_3$ 10, trehalose 5, sucrose 30, HEPES 5, pH7.2; (Verstreken et al., 2008)] and then stimulated for 5 min with 60 mM KCl and 5 mM $CaCl_2$ in HL-3 saline with reduced NaCl concentration to adjust the osmolarity. Afterwards, larvae were washed with calcium-free HL-3 for 5 min and fixed with 4% PFA and 0.5% glutaraldehyde for 10 min at RT followed by 2% glutaraldehyde for 1h at RT (all fixatives where prepared in 0.1M sodium cacodylate buffer, pH7.2). After washing osmification was performed with 1% osmium tetroxide and 0.8% KFeCn followed by en bloc staining with 1% uranyl acetate in distilled water for 1 h. Following dehydration with ethanol, samples were infiltrated in Epon resin. For embedding muscle 6 and 7 of segment 2-5 were cut out and positioned as a stack on an Epon dummy for high throughput analysis followed by hardening overnight at 60°C. 55-60 nm sections were obtained and stained with uranyl acetate/lead citrate following standard protocol. Micrographs of neuromuscular junctions were taken at x30000 magnification in transmission electron microscope (EM 902A; Zeiss). Morphometric analysis was performed with Image J.

Synapto-pHluorin imaging

Imaging of synapto-pHluorin (SpH) was performed as described previously (Poskanzer et al., 2006). All SpH experiments were carried out using an upright epifluorescence Olympus BX51WI microscope equipped with a Hamamatsu Orca ER cooled CCD digital camera and a Visitron Lambda DG-4 illumination system, with a 40x water immersion lens under control of Metafluor Ver 6.1 software (Molecular Devices Corporation, Downingtown, PA USA). Boutons in muscle 6/7 of A2 or A3 segment were analyzed. Animals were bathed in HL-3 with 5 mM $CaCl_2$ and 100µM 1-Naphthylacetyl spermine trihydrochloride (a glutamate receptor blocker to suppress muscle contractions, Sigma). Experiments in the presence of

folimycin (Sigma) were done at a final concentration of 134 nM in HL-3. Image series were acquired at 2 Hz and the specific SpH fluorescence within a bouton at each time point was obtained by measuring the integrated fluorescence intensity of a region of interest (ROI) surrounding the bouton and by subtracting the integrated intensity of a background-region within a ROI of identical dimensions. The mean fluorescence intensity prior to electrical stimulation (corresponding to the first 10 frames) was subtracted from each trace, the curves were then divided by their maximal fluorescence value and subsequently averaged to obtain the $\Delta F/F_{max}$-curves depicted in Figure 4 H and I. Kinetic analysis was performed on individual traces. The function $f(t)=Amp_{fast}*exp(-(t-t_0)/\tau_{fast})+Amp_{slow}*exp(-(t-t_0)/\tau_{slow})$ was fit to the fluorescence decay using the CurveFit function of IGOR Pro (6.22A, Wavemetrics).

Supplementary references

Bushlin, I., Petralia, R.S., Wu, F., Harel, A., Mughal, M.R., Mattson, M.P., and Yao, P.J. (2008). Clathrin assembly protein AP180 and CALM differentially control axogenesis and dendrite outgrowth in embryonic hippocampal neurons. J Neurosci *28*, 10257-10271.

Göttfert, F., Wurm, C.A., Mueller, V., Berning, S., Cordes, V.C., Honigmann, A., and Hell, S.W. (2013). Coaligned dual-channel STED nanoscopy and molecular diffusion analysis at 20 nm resolution. Biophys J 105, L01-03.

Kittel, R.J., Wichmann, C., Rasse, T.M., Fouquet, W., Schmidt, M., Schmid, A., Wagh, D.A., Pawlu, C., Kellner, R.R., Willig, K.I*., et al.* (2006). Bruchpilot promotes active zone assembly, Ca2+ channel clustering, and vesicle release. Science *312*, 1051-1054.

Kuromi, H., Yoshihara, M., and Kidokoro, Y. (1997). An inhibitory role of calcineurin in endocytosis of synaptic vesicles at nerve terminals of Drosophila larvae. Neuroscience research *27*, 101-113.

Lampe, A., Haucke, V., Sigrist, S.J., Heilemann, M., and Schmoranzer, J. (2011). Multi-Color Direct STORM with Red Emitting Carbocyanines. Biol Cell.

Owald, D., Fouquet, W., Schmidt, M., Wichmann, C., Mertel, S., Depner, H., Christiansen, F., Zube, C., Quentin, C., Korner, J.*, et al.* (2010). A Syd-1 homologue regulates pre- and postsynaptic maturation in Drosophila. J Cell Biol *188*, 565-579.

Phillips, G.R., Huang, J.K., Wang, Y., Tanaka, H., Shapiro, L., Zhang, W., Shan, W.S., Arndt, K., Frank, M., Gordon, R.E.*, et al.* (2001). The presynaptic particle web: ultrastructure, composition, dissolution, and reconstitution. Neuron *32*, 63-77.

Poskanzer, K.E., Fetter, R.D., and Davis, G.W. (2006). Discrete residues in the c(2)b domain of synaptotagmin I independently specify endocytic rate and synaptic vesicle size. Neuron *50*, 49-62.

Qin, G., Schwarz, T., Kittel, R.J., Schmid, A., Rasse, T.M., Kappei, D., Ponimaskin, E., Heckmann, M., and Sigrist, S.J. (2005). Four different subunits are essential for expressing the synaptic glutamate receptor at neuromuscular junctions of Drosophila. J Neurosci *25*, 3209-3218.

Ramaswami, M., Krishnan, K.S., and Kelly, R.B. (1994). Intermediates in synaptic vesicle recycling revealed by optical imaging of Drosophila neuromuscular junctions. Neuron *13*, 363-375.

Sigrist, S.J., Reiff, D.F., Thiel, P.R., Steinert, J.R., and Schuster, C.M. (2003). Experience-dependent strengthening of Drosophila neuromuscular junctions. J Neurosci *23*, 6546-6556.

Stewart, B.A., Atwood, H.L., Renger, J.J., Wang, J., and Wu, C.F. (1994). Improved stability of Drosophila larval neuromuscular preparations in haemolymph-like physiological solutions. Journal of comparative physiology *175*, 179-191.

Verstreken, P., Ohyama, T., and Bellen, H.J. (2008). FM 1-43 labeling of synaptic vesicle pools at the Drosophila neuromuscular junction. Methods Mol Biol *440*, 349-369.

Walther, K., Diril, M.K., Jung, N., and Haucke, V. (2004). Functional dissection of the interactions of stonin 2 with the adaptor complex AP-2 and synaptotagmin. Proc Natl Acad Sci U S A *101*, 964-969.

Wienisch, M., and Klingauf, J. (2006). Vesicular proteins exocytosed and subsequently retrieved by compensatory endocytosis are nonidentical. Nat Neurosci *9*, 1019-1027.

Wolter, S., Schuttpelz, M., Tscherepanow, M., S, V.D.L., Heilemann, M., and Sauer, M. (2010). Real-time computation of subdiffraction-resolution fluorescence images. Journal of microscopy *237*, 12-22.

Zhang, H., Webb, D.J., Asmussen, H., Niu, S., and Horwitz, A.F. (2005). A GIT1/PIX/Rac/PAK signaling module regulates spine morphogenesis and synapse formation through MLC. J Neurosci *25*, 3379-3388.